ECG BASELINE WANDER CORRECTION AND NOISE REDUCTION

A dissertation submitted in

partial fulfillment of the requirements for the degree of

Master of Technology

by

P. Mithun

Roll Number 08330011

Under the supervision of

Prof. P. C. Pandey

Department of Biosciences and Bioengineering

Indian Institute of Technology Bombay

June 2010

Indian Institute of Technology Bombay

M. Tech Dissertation Approval

This dissertation entitled "ECG baseline wander correction and noise reduction" by P. Mithun (Roll No. 08330011), is approved for the degree of Master of Technology in Biomedical Engineering.

Supervisor : ______________________ (Prof. P. C. Pandey)

Examiners : ______________________ (Prof. S. Mukherji)

: ______________________ (Prof. S. Chaudhuri)

Chairman : ______________________ (Prof. Preeti Rao)

Date : 29th June 2010

Declaration

I declare that this written submission represents my ideas in my own words and where others' ideas or words have been included, I have adequately cited and referenced the original sources. I also declare that I have adhered to all principles of academic honesty and integrity and have not misrepresented or fabricated or falsified any idea/data/fact/source in my submission. I understand that any violation of the above will be cause for disciplinary action by the Institute and can also evoke penal action from the sources which have thus not been properly cited or from whom proper permission has not been taken when needed.

(P. Mithun)

Date: 29th June 2010

P. Mithun / Prof. P. C. Pandey (Supervisor), “ECG baseline wander correction and noise reduction”, *M. Tech. dissertation*, Biomedical Engineering Group, Department of Biosciences and Bioengineering, Indian Institute of Technology Bombay, June 2010.

ABSTRACT

The project objective is to investigate methods for correcting motion artifact and baseline wander. Out of the various denoising methods reviewed, the wavelet-based denoising using scale-dependent thresholding was investigated. The decomposition levels containing negligible amount of signal and significant noise were removed and the signal was reconstructed. The wavelets Daubechies 8 (db8) and discrete Meyer (dmey) performed better than the other wavelets studied. From the study conducted on ECG signals from various sources, it was observed that the investigated technique suppresses the baseline wander significantly and it improved automated detection of R-peaks. A FIR band-pass filter was designed to approximate the filtering by wavelet-based denoising and it gave a comparable performance.

CONTENTS

List of Figures

Chapter 1
INTRODUCTION

1.1 Problem overview

Electrocardiogram (ECG) is a projection of the electric potentials developed by the heart which is obtained by placing electrodes on specific locations of the skin [1]-[3]. Various kinds of disturbances affect the sensing, amplification, and recording of these signals. The characteristic of the disturbances and how they affect the ECG depend on their sources. The disturbances related to human activity are known as artifacts. There are three main sources of artifacts: (a) other electric potentials inside the body, (b) potentials generated at the skin-electrode interface, and (c) offset and drift in the amplifier.

The interference in the ECG due to other electric signals generated inside the body primarily consists of the myopotentials, the electric signals produced by the skeletal muscles during their contraction. The myopotential (electromyogram noise or the EMG noise) severely affects the ECG because of the overlap in their spectra. The ECG spectrum extends from 0.01 Hz to 250 Hz and the myopotential spectrum extends from 0 to 10 kHz [2], [3]. The level of the noise depends on the closeness of the myopotential origin to the electrodes. The electric potentials in the brain and eye are not strong enough to contaminate the ECG signal. Another source of interference is due to coupling of the mains voltage to the body as picked-up by the ECG electrodes, known as the powerline interference. It can be reduced by a careful design of the ECG acquisition system, and can be suppressed by filtering.

Electric potentials at the skin-electrode interface are another source of artifacts. The electrode movement causes a change in the interface impedance which causes distortion in the signal in the form of amplitude modulation. This can be minimized by using high input impedance amplifiers. The electrode motion also causes changes in its half-cell potential. The difference in the half-cell potentials at

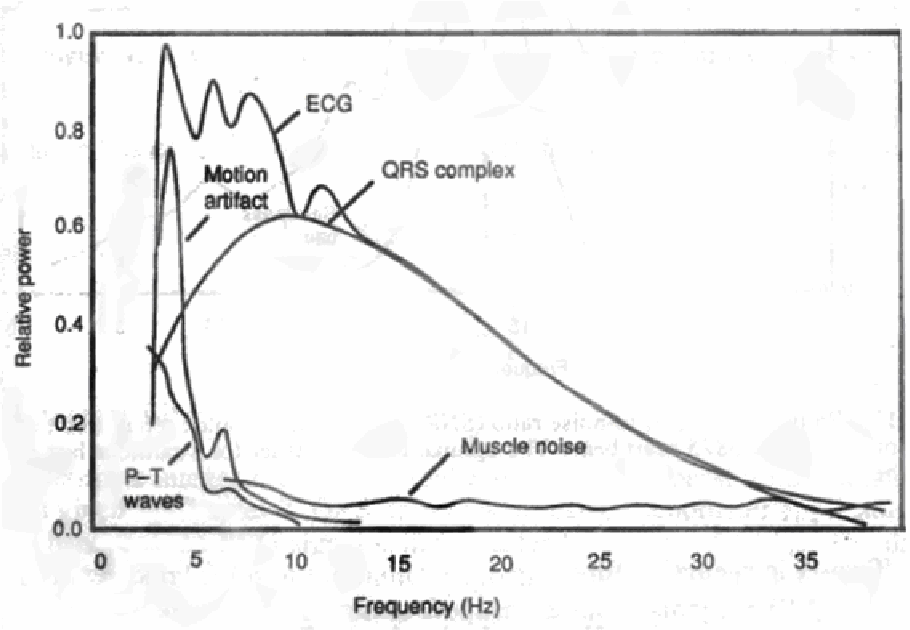

Fig. 1.1. Relative power spectra of QRS complex, P and T waves, muscle noise, and motion artifacts based on an average of 150 beats [3].

the electrodes gets amplified by the ECG sensing amplifiers, causing irregular baseline wander in the final ECG, known as motion artifact [3]-[5]. The spectrum of motion artifacts and myopotential noise overlap with that of ECG. At times, the shape of the motion artifact looks similar to that of P wave or R wave. Variations in temperature and pressure at the skin-electrode interface also introduce baseline wander in ECG signals. It is a slow-varying noise, in the order of 0 to 1 Hz [3], [6]. The DC offset and drift in the amplifier also contribute to the baseline wander in the ECG signal. Digitization of the ECG introduces quantization error, which may be modeled as a broad-band noise.

The approximate relative power spectra of the ECG, QRS complex, P and T waves, motion artifact, and EMG noise [3], given in Fig. 1.1 indicate relative strengths and overlaps. The artifacts in ECG make it difficult to detect the P wave, time interval between the characteristic points, elevation or dip of the ST segment from the isoelectric levels, etc. The QRS complex detection algorithms face problems in the presence of significant baseline wander and motion artifact. The performance of most of the automated feature extraction and signal compression algorithms also gets affected by the artifacts [5]-[10]. The motion artifacts can be minimized by restricting the motion of the patients during signal recording, but this is not feasible in ambulatory ECG recording, and hence denoising is particularly important in clinical use of ambulatory ECG signals.

1.2 Project objective

The aim of this project is to investigate denoising techniques for suppressing motion artifacts and baseline wander from the ECG signals obtained from a Holter ECG monitor. The denoising method should not need any reference input, and automated QRS detection should be feasible after denoising the ECG signal. A review of the literature showed the wavelet-based denoising technique to have properties matching the above objectives and hence it has been selected for a detailed investigation.

1.3 Report outline

Chapter 2 presents a review of various techniques for denoising of ECG and some other biosignals. The investigations on the denoising method are described in Chapter 3. Chapter 4 presents the details of validation procedures used and the results obtained. A summary of the work done and some suggestions for future work are given in the last chapter.

Chapter 2
ECG DENOISING TECHNIQUES

2.1 Introduction

This chapter gives a review of some of the ECG denoising techniques: linear filtering, adaptive filtering, non-linear filtering techniques (independent component analysis, mathematical morphology filtering, and moving window averaging), and denoising techniques based on wavelets and empirical mode decomposition.

2.2 Filtering based ECG denoising techniques

A technique for removing the baseline wander and the power line interference by linear filtering was reported in [11], with main focus on reducing the computational complexity. It used a fixed cutoff frequency FIR filter for the input signal sampled at 250 Hz. Assuming the minimum beat rate to be 48 beats per minute, the lowest frequency content in the ECG was taken as 0.8 Hz. The cutoff frequency was set to 0.7 Hz as the lower cutoff frequency needed a larger number of filter coefficients. Selecting the filter taps at delays of 1/50 s resulted in a stop-band of 1.4 Hz at the harmonics of 50 Hz. It was reported that the same filter could be used to remove 60 Hz interference by sampling the input ECG at 360 Hz. As no periodicity matching with the heartbeat was observed in the difference between input and output signals, it was concluded that filtering did not result in a loss of the spectral components of the ECG signal.

The spectrum of baseline wander in ECG varies with time. Pandit [6] used a high pass filter with variable cut-off frequency to filter out the baseline wander in the 0 – 1 Hz range. The predominant component in 0 – 1 Hz range in the short-time Fourier transform (STFT) of the input ECG was taken as the predominant component of the baseline wander. This frequency was used to decide the cutoff frequency of the high pass filter. A window size of 4 s or larger was required for good spectral resolution in the 0 – 1 Hz range.

The powerline noise can be suppressed by a notch filter. For removing myopotential noise, motion artifacts, and baseline wander which have a significant spectral overlap with ECG, adaptive filtering techniques have been reported [4], [12]. Adaptive filter uses an adaptive algorithm which dynamically changes the filter coefficients to minimize the mean square error between the filtered reference and the input signal.

Thakor and Zhu [12] used adaptive filtering for reducing baseline wander, 60 Hz powerline noise, EMG noise, and motion artifacts from the ECG signal sampled at 500 Hz. To remove the baseline wander, a notch filter with the notch at zero frequency was realized by applying a constant value as the reference for adaptive filtering and only one filter coefficient for minimizing the error output. The frequency components up to 0.5 Hz were removed. However, there was a distortion in the ST segments of the denoised ECG. As the common mode drive to the reference electrode (right leg) contains no ECG, it was used as the reference for adaptive filtering of the powerline noise. The advantage of this method, over simple notch filtering, is that the useful components in the ECG signal near to 60 Hz can be retained. The EMG noise was handled using multilead ECG, assuming the EMG noises in different leads to be uncorrelated. The augmented lead aVF was used as the primary input, with the orthogonal vector aVR – aVL as the reference input, for cancelling the correlated ECG and resulting in the uncorrelated EMG noise as the error output. For motion artifact cancellation, ECG signal with motion artifact was used as the primary input, with impulses located at the beginning of the P waves as the reference input. The length of the filter spanned the P-QRS-T complex. During filtering, the adaptation takes place only for the samples which represent the P-QRS-T complex. Subtracting this complex from the noisy ECG leaves the motion artifact as residue. It was reported that denoised ECG was useful only for heart rate measurements and arrhythmia detection. A major problem with the method is that the length of the P-QRS-T complex cannot be considered constant in ambulatory ECG, particularly during arrhythmia. Further, it is generally difficult to detect the P wave, particularly in the ECG contaminated by motion artifact.

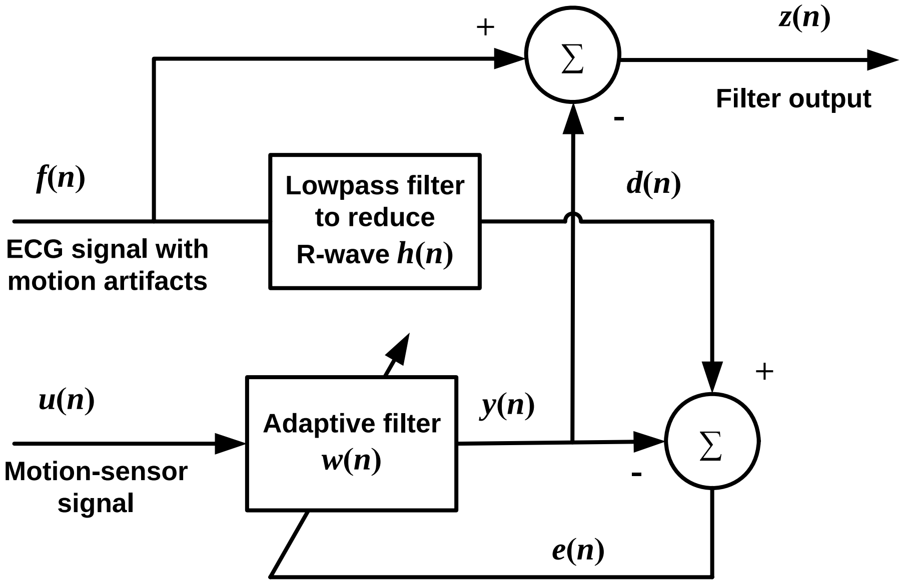

Fig. 2.1. Adaptive filtering scheme of [4] using motion sensor

In the motion artifact cancellation scheme presented in [4], a motion sensor was placed on the ECG electrode on the left arm to detect the movement electrode. The motion sensor output was used as the reference, as shown in Fig. 2.1. Least mean square (LMS) algorithm was used to adjust the filter coefficients vector **w** for minimizing the error $e(n)$. As the reference is correlated with the motion artifact, and uncorrelated with the ECG signal, the filtered output $y(n)$ is expected to closely represent the motion artifact. Subtracting $y(n)$ from noisy ECG input $f(n)$ gives the denoised signal $z(n)$. To improve adaptation, the input ECG was lowpass filtered to reduce the R-wave in the primary input $d(n)$. To validate the method, first ECG was recorded without any motion artifact. Then a recording was made from the same patient under similar circumstances, while pushing and pulling the electrode, and pushing the skin around the electrode, for introducing motion artifacts. The noisy ECG signal was filtered using the adaptive filter. The effectiveness of filtering was quantified by calculating the L_2 norm and MaxMin statistic. For a waveform $x(n)$, the statistics were defined as

$$L_2\left\{x(n)\right\} = \sqrt{\sum_{\text{all } n} x(n)^2} \tag{2.1}$$

$$L_{\text{mxmn}}\left\{x(n)\right\} = \max_{\text{all } n}\left[x(n)\right] - \min_{\text{all } n}\left[x(n)\right] \tag{2.2}$$

The statistics were calculated for the noisy signal before filtering, after filtering, and the ECG recorded without motion artifact. Improvement indices for L_2 and L_{mxmn} were calculated as

$$\text{Improvement} = \frac{\left|(\text{Pre-filtering statistic}) - (\text{Post-filtering statistic})\right|}{\left|(\text{Pre-filtering statistic}) - (\text{Artifact-free statistic})\right|} \qquad (2.3)$$

The filter performance depended on the sensor used, with 79 – 91% improvement in L_2 norm statistic, and 49 – 67% improvement in MaxMin statistic. A limitation of the method appears to be that it can be applied for reducing the motion artifact due to one electrode only.

2.3 Denoising by nonlinear filtering

A method based on independent component analysis (ICA) for separating the ECG signal and the noise is reported in [5]. ICA can be used to separate a signal into *m* independent components using *m* simultaneous observations of the signal. Let **S** be a vector of *m* statistically independent components, and let *m* simultaneous observations which are linear combinations of these components be written as

$$\mathbf{X} = \mathbf{AS} \qquad (2.4)$$

where **A** is an unknown matrix of order $m \times m$, representing the mixing. The ICA involves finding a matrix **U** to undo the mixing effect,

$$\mathbf{V} = \mathbf{UX} \qquad (2.5)$$

where **V** is an estimate of **S**. The authors used an algorithm named JADE (Joint

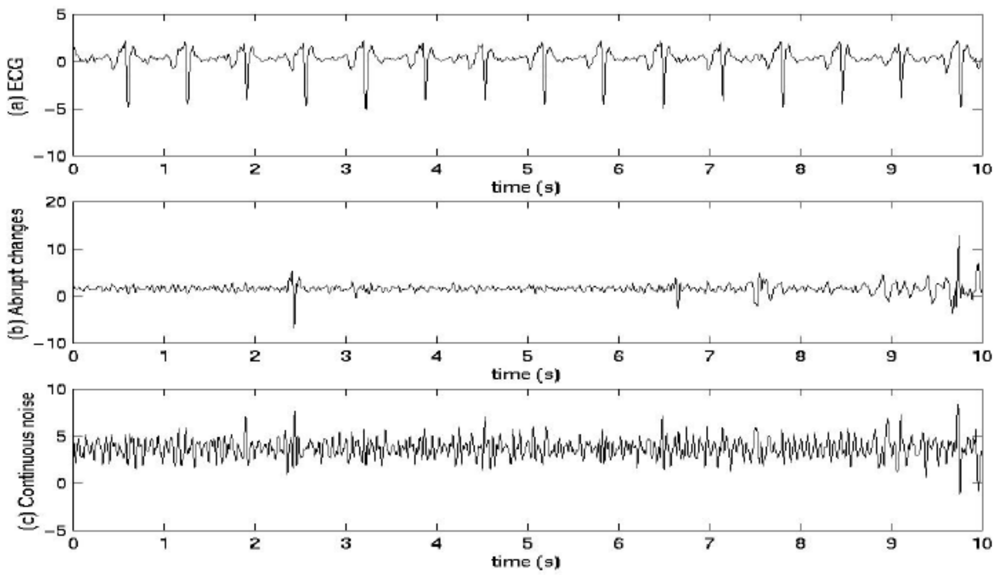

Fig 2.2. Typical waveforms of independent components which represent (a) the ECG, (b) abrupt changes, and (c) continuous noise [5]

Approximate Diagonalization of Eigen matrices) which has been reported to give good results when the number of observations is small. They applied ICA on 3-lead ECG as the input and estimated three components as the output. It was observed that the ECG signals and the noise were represented by different independent components. The components representing noise were located, and set to zero and the remaining components were mixed back to get the denoised set of observations

$$\mathbf{X}' = \mathbf{U}^{-1}\mathbf{V}' \tag{2.6}$$

It was found that the noise could be represented by first, second, or third component, and hence a visual inspection was required to determine the component representing noise.

Mainly three types of components were possible: the ECG signal, abrupt changes, or continuous noise. Examples for each type are shown in Fig. 2.2. The authors used kurtosis to find the components representing continuous noise. Kurtosis of a signal $\mathbf{x}$ is given as

$$\mathrm{Kurt}(x) = \mathrm{E}(x^4) - 3\left[\mathrm{E}(x^2)\right]^2 \tag{2.7}$$

It is zero for Gaussian densities and large for signals with probability density deviating from the Gaussian. Since the continuous noise has a distribution closer to Gaussian, its kurtosis is closer to zero. The Kurtosis value of ECG and of the abrupt changes is large. The component representing continuous noise was detected using a suitable threshold for the kurtosis value. The presence of abrupt changes was determined using the variance. The components were divided into small sections, each of 1 s. The variance of each section was computed. The sections with large variance were taken to be abrupt. The ECG and the continuous noise have comparatively constant variance for all the sections. The variability of the section variances was measured using the variance of the section variances, denoted by $\mathrm{Var}_{\mathrm{var}}$. If this quantity was very high for a component, it was taken to represent abrupt changes.

The authors validated the method using clinical recordings, obtained using 3 electrodes placed on right hand (RA), left leg (LL), and chest (V5). The voltages were used to get three channel output. Two channels represented ECG lead II and V5. The third channel didn't have any clinical significance. The ground was taken to be the average of the three channels. The acquired signals were filtered using high pass and lowpass FIR filters with cutoff frequencies 1 Hz and 40 Hz respectively. The filtered signals were processed using JADE algorithm to separate the three independent components. The noise components were identified using kurtosis and Var_{var} indices. The identified noise components were set to zero, and the ECG was reconstructed using Eq. 2.6. It was observed that the components representing noise were identified successfully using the automated algorithm based on Kurtosis and Var_{var}. Also, there were no visible distortions to the actual ECG signal.

Curve-fitting methods have also been used to estimate and suppress the baseline wander. Meyer and Keiser [13] located the PR segment of the ECG signal using a second order estimator. Taking the located PR segment points as knots, a third order cubic spline curve was used to get an estimate of the baseline and was subtracted from the observed signal to get the baseline corrected signal. The method was applied on an ECG obtained from a treadmill exercise on which a computer generated baseline noise was added to simulate the baseline wander. For the heart rate of 60 beat/min, the baseline noise components of frequencies up to 0.25 Hz were effectively removed without affecting the ST segment and for the heart rate of 150 beat/min, the noise components up to 0.6 Hz were removed. The better performance for higher heart beats was attributed to the closer placing of the knots and hence better approximation by the cubic spline curve. However, detecting the knots in the presence of noises like motion artifact or EMG noise is a hurdle faced by this method.

Mathematical morphology filter is a nonlinear filter that makes use of the shape information of the signal to separate it from the noise. Chu and Delp [14] used, two basic morphology operators, erosion and dilation, for the reduction of background noise, impulsive noise, and baseline wander. Erosion for the input sequence *f*(*m*) of length *N* is defined as,

$$(f \ominus k)(m) = \min_{n=0,\ldots,M-1} \{ f(m+n) - k(n) \}, 0 \le m \le N-m \tag{2.8}$$

where k is a predefined function of length M called the structural element (SE). Similarly, dilation is defined as

$$(f \oplus k)(m) = \max_{n=m-M+1,\ldots,m} \{ f(n) + k(m-n) \}, m-1 \le m \le N-1 \tag{2.9}$$

Two higher level operations called opening, denoted by '$\circ$' and closing, denoted by '$\bullet$', are defined as follows:

$$(f \circ k)(m) = ((f \ominus k) \oplus k)(m) \tag{2.10}$$

$$(f \bullet k)(m) = ((f \oplus k) \ominus k)(m) \tag{2.11}$$

Conceptually, opening operation eliminates peaks occurring within *M* samples and, closing removes dips occuring within *M* samples. The block diagram of the algorithm to suppress the high frequency noises and baseline wander is shown in Fig. 2.3. A dome shaped structural element with length 5 was used to remove the impulsive noise and the high frequency background noise. The dome-shaped structural element helped in minimizing the R-peak height reduction. To estimate the baseline wander, two structural elements of lengths 41 and 81 were used. With the input ECG sampled at 360 Hz, these operations eliminated the dips and peaks within 113.88 ms. leaving the baseline of the input ECG. Reversing the order of opening and closing operations and taking the average improved the output.

The method was first evaluated using simulation studies. Clean ECG from an analog ECG simulator was digitized at a sampling rate of 1 kHz using 12-bit

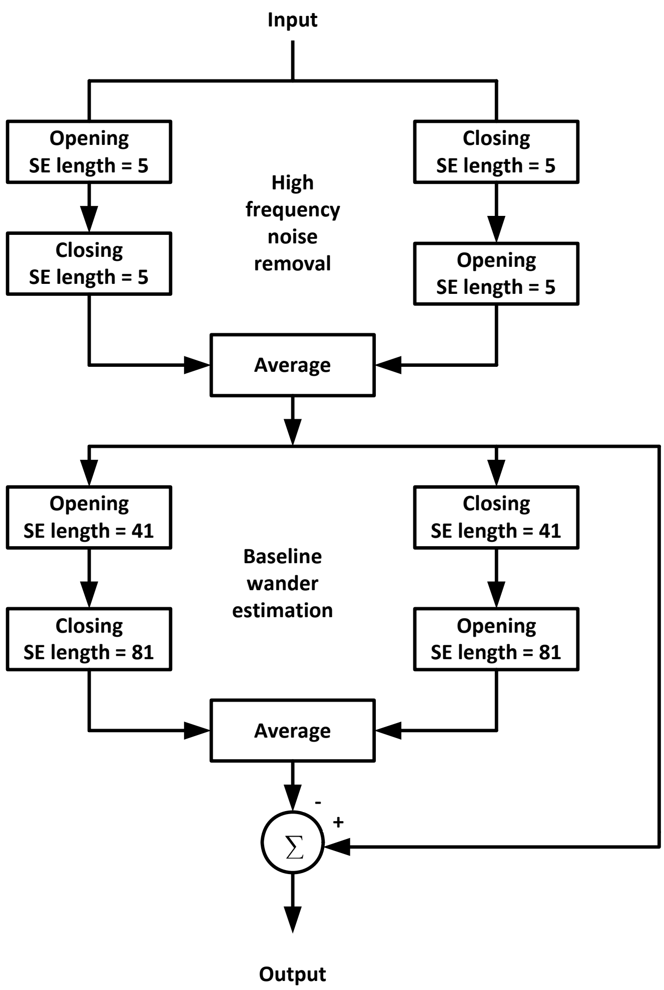

Fig 2.3. Mathematical morphology filtering algorithm used in [14] to remove high frequency noise and baseline wander removal from ECG signals.

quantification. A Gaussian noise was added to simulate the background noise. Impulse noise was generated using another Gaussian noise of variance 2 to 20 times the variance of the background noise. Baseline wander consisted of a sinusoid added to a slanting line. The RMS error in the noisy ECG, and the processed ECG with reference to the clear ECG were calculated as percentage of the peak to peak value of the clean ECG. The processing reduced the RMS error from 30 – 40% to 4 – 4.5%. A shorter length of the structural element improved the performance. The variations in the shape and the height of the structural element did not have any effect. A higher sampling rate improved the denoising. After selecting the parameters on the basis of simulation results, the authors applied the processing on using clinical recordings from the MIT/BIH arrhythmia database. The processing did not cause any distortions in the ECG signal, except slight distortion in the ST segment.

The problem faced by Chu and Delp's [14] method in baseline wander reduction has been addressed by Sun *et al.*[15] in their attempt to remove baseline wander from neonatal ECG signals. The authors attributed the degradation of performance of morphological filtering to the following two facts.

a) If the structural element width is more than PR interval, the PR interval may not be restored to isoelectric level.
b) If the width of the structural element is less than the width of the T wave, a residue of the T wave may remain even after the morphology operations.

Figure 2.4 explains the above mentioned facts. The problems were solved by removing the QRS complexes from the input ECG. Morphology filtering using a flat (all zero) structural element of width 69 ms, removed QRS complex from ECG signal. The residual signal, which contain the P wave, T wave and the baseline wander was

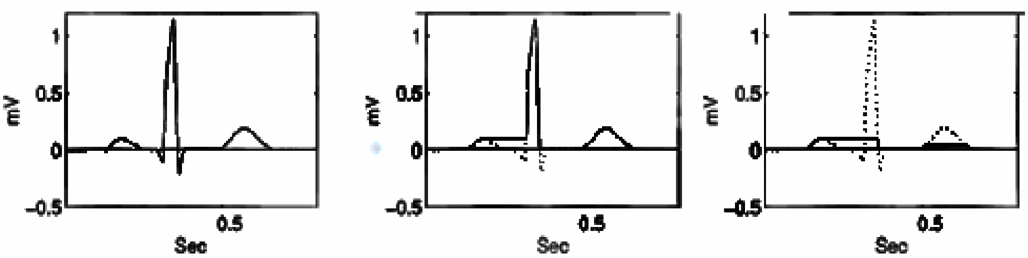

Fig. 2.4. Problems in the estimation of baseline as shown in [15]. Left to right: input ECG signal; after opening operation using a SE of length more than PR interval; after closing operation with SE less than the T wave duration.

further filtered using morphology filtering. The structural element used had a width equal to the QT interval, with all zero samples. The SNR improvement achieved by the modified method was approximately 6 dB higher than that achieved by the earlier method. The method was further validated using clinically recorded ECG signals, by measuring the standard deviations of amplitudes of R waves, P waves, T waves, and ST segments from the normalized ECG output. The standard deviations of RR, PR, QRS, and QT intervals were also calculated. As compared to the earlier method, the modified method resulted in equal or smaller standard deviations for all the parameters.

Dai and Lian [7] used a modified moving window averaging to estimate and remove baseline wander from ECG records. Window averaging can be seen as a lowpass filtering operation. With a rectangular window of size N, the estimated baseline $y(n)$ for input ECG $x(n)$ is estimated as

$$y(n) = \frac{1}{N}\sum_{i=0}^{N-1} x(n-i) \tag{2.12}$$

To reduce the ECG component in the estimated baseline, two modifications were made to the traditional moving average. One modification was to take the moving average of samples separated by intervals rather than continuous samples.

$$y(n) = \frac{1}{N}\sum_{i=0}^{N-1} x(n-is) \tag{2.13}$$

where s is the interval step. In case of higher sampling rate, a correspondingly higher value of s needs to be chosen. The second modification was to remove the samples corresponding to the R wave from the expression. If the k^{th} sample of the input was representing a part of R wave, Eq. 2.13 is modified as,

$$y(k) = \frac{1}{N-1}\sum_{i=1}^{N-1} x(k-is) \tag{2.14}$$

The method was validated using a clean record from MIT/BIH arrhythmia database. The baseline was simulated using a combination of sine and cosine waves of 0.2 Hz. The performance was evaluated using correlation coefficient between the actual clean ECG and the denoised output. Use of the modifications improved the correlation from 0.854 to 0.965.

2.4 Denoising methods based on wavelets

Wavelet-based processing is one of the most commonly used signal denoising technique. A wavelet is an oscillation lasting for a small duration and satisfying the following criteria:

a) The mean value of the function is zero.

b) The norm of the function is unity.

c) The function is orthogonal to its translated and/or scaled versions.

A prototype of the wavelet is called the mother wavelet. A waveform can be represented as a linear combination of shifted and scaled versions of the mother wavelet [16]-[18]. The wavelet transform $W(m,n)$ on the input waveform $x(t)$ is defined as

$$W(m,n) = \int_{-\infty}^{\infty} x(t)\Psi^{*}_{m,n}(t)dt \tag{2.15}$$

where $\Psi_{m,n}(t)$ is the dilated and shifted version of the mother wavelet $\Psi(t)$ as per the equation,

$$\Psi_{m,n}(t) = 2^{-m/2}\Psi(2^{-m}t - n) \tag{2.16}$$

The values of $W(m,n)$ for a given m are known as the wavelet detail coefficients at scale m. The original waveform can be recovered back using the inverse wavelet transform given by

$$x(t) = \sum_{m=1}^{\infty}\sum_{n=-\infty}^{\infty} W(m,n)\Psi_{m,n}(t) \tag{2.17}$$

Using the wavelet coefficients at scale m, the input waveform is represented as waveform approximation $\mathbf{A}_m$ and waveform detail $\mathbf{D}_m$ as

$$D_m(t) = \sum_{n=-\infty}^{\infty} W(m,n)\Psi_{m,n}(t) \tag{2.18}$$

$$A_m(t) = A_{m-1}(t) - D_m(t) \tag{2.19}$$

A schematic representation of the wavelet decomposition is shown in Fig. 2.5. The detail and approximation in each scale represent a specific frequency band. Lower scale details represent higher frequencies with lower frequency resolution, while higher scale details represent lower frequencies with higher frequency resolution. At a given scale, the approximation represents a lowpass filtered version of the original waveform. The cutoff frequency of the lowpass filter is equal to the lower frequency

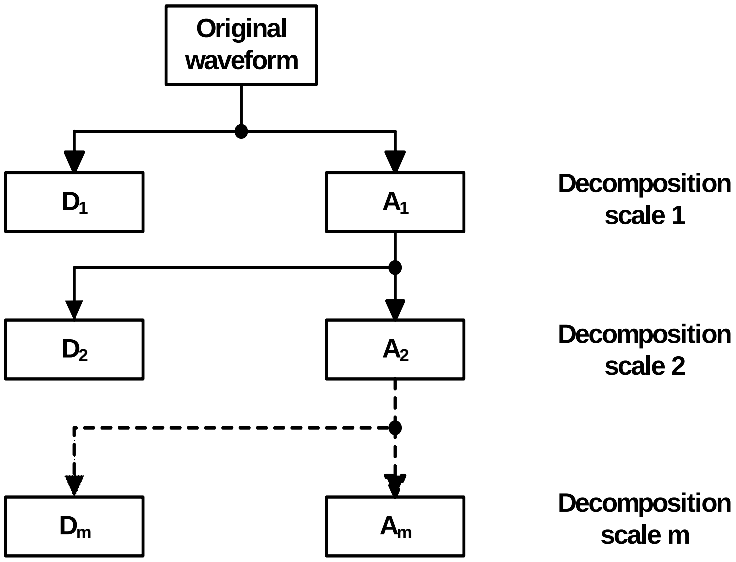

Fig. 2.5. Block diagram showing the wavelet decomposition levels. D_m and A_m are the m^{th} level detail and approximation of the original waveform respectively.

bound of the detail in the same scale. For the sampling rate of f_s, the lower and upper frequency bounds of the m^{th} scale detail are given approximately by

$$f_{\mathrm{L}} \approx \frac{f_{\mathrm{s}}}{2^{m+1}} \tag{2.20}$$

$$f_{\mathrm{H}} \approx \frac{f_{\mathrm{s}}}{2^{m}} \tag{2.21}$$

A large number of wavelet families have been investigated and compactness of the wavelet representation of a waveform depends on the similarity of the waveform with the wavelet.

A wavelet-based approach has been reported in [19] and [20] to remove the baseline wander from the pulse waveform. The discrete Meyer wavelet was used to decompose the input waveform in 6 scales. The discrete Meyer wavelet has a smooth shape, suitable for representing the smooth pulse waveform. It was observed that the 6^{th} scale approximation closely represents the baseline wander. With the sampling rate of 100 Hz, the 6^{th} scale approximation contained frequencies up to about 0.68 Hz. The baseline approximation was subtracted from the input signal to get the denoised signal. Application of the processing on input signals with different levels of contamination showed that if the baseline wander present was small, the wavelet processing resulted in distortions in the pulse signal. The distortions were negligible if the input had high levels of noise. A spline interpolation was used to further correct the signal. The onsets of the pulse waveform were given as the knot sequence for the interpolation using a cubic spline curve. The resulting curve represented the baseline of the input wave. However, the performance of the spline interpolation was poor if the baseline wander present in the signal was high. Hence the denoising technique was chosen according to the level of baseline wander present in the signal. A quantity called the energy ratio (ER) was used to measure the level of the baseline wander present in the signal. and defined using the first and sixth level approximations ($\mathbf{A}_1$ and $\mathbf{A}_6$) as,

$$\text{ER}=20\log_{10}\frac{\left\|\mathbf{A}_1-\text{mean}(\mathbf{A}_1)\right\|}{\left\|\mathbf{A}_6-\text{mean}(\mathbf{A}_6)\right\|} \tag{2.22}$$

If the input signal had an ER > 50, the baseline was removed using spline interpolation alone. Otherwise the wavelet filtering was implemented first by subtracting the 6$^{\text{th}}$ scale approximation from the input signal followed by correction using spline interpolation. It was reported that the baseline correction achieved by the ER based processing performed better than that achieved by the previously developed methods based on FIR filtering, spline interpolation, and mathematical morphology filtering. for removal of the baseline drift in the pulse waveform.

Another instance of wavelet-based baseline wander reduction can be seen in [21] for removing the respiratory artifact from the impedance cardiography (ICG) signal. The respiration causes significant baseline wander in the ICG waveform. The decomposition of the artifact-free ICG signal, sampled at 500Hz, using discrete Meyer wavelet showed that the ICG can be completely represented by details of first 8 scales. When ICG-free artifact was analyzed using the same wavelets, it was noticed that 10 scales of decomposition was required to completely represent it. It was also noticed that the first 8 scales of details doesn't contain significant components of the ICG-free artifact. Hence the signal was decomposed into 10 scales using discrete Meyer wavelet, and the signal was resynthesized by adding the first 8 scale details only. The processing was first tested on noisy input, simulated by adding signal-free artifact $r_0(n)$ to artifact-free signal $s(n)$

$$x(n)=s(n)+\alpha r_0(n) \tag{2.23}$$

where α is the mixing ratio. The signal to noise ratio at the input was obtained as,

$$\text{SNR} = -20\log\alpha \tag{2.24}$$

and a measure of SNR at the output, called the signal to error ratio (SER) was obtained as

$$\mathrm{SER} = 10\log\left(\frac{\sum_{i=1}^{N} s^2(i)}{\sum_{i=1}^{N}\left|\hat{x}(i)-s(i)\right|^2}\right) \tag{2.25}$$

where $\hat{x}(n)$ is the denoised output. The processing achieved an average SNR improvement of 21.8 dB for the input SNR of –9 to 9 dB. Validation of the processing using clinically acquired ICG data showed that the denoised ICG can be used for estimating the stroke volume on beat-by-beat basis.

Wavelet-based denoising methods have been applied in the context of ECG denoising also [22]-[26]. Zhang removed the baseline wander from the ECG signal, sampled at 360 Hz, by subtracting its 8th scale approximation ($\mathbf{A}_8$) obtained from wavelet decomposition [22]. The wavelet used was Symlets order 10, because its shape similarity to the QRS complex. The method was validated using synthesized signal obtained by adding a clean ECG record with a record of baseline wander, both from the MIT/BIH database. The added baseline wander was best approximated by $\mathbf{A}_8$ (containing frequencies up to 0.7 Hz). It was reported that this method caused distortions in the slow varying ST segments.

When a noisy signal is decomposed using wavelets, it is possible that a particular detail contains both signal and noise components. In such circumstances, the true signal component can be separated from the noise using a method called wavelet thresholding [23], [24]. These methods are based on the following assumptions:

a) The noise is uniformly distributed in the time domain and it has low amplitude.
b) The signal information is concentrated in specific time instances and it is high in amplitude.

High frequency noise is generally located at initial scales. If the wavelet coefficients are analyzed in those initial scales in which both the signal and noise information is present, under the above mentioned assumptions, the noise part of the input is represented by low valued wavelet coefficients and is distributed uniformly. The coefficients representing the true signal will be located at specific instances and will have high amplitude. Hence, by applying a suitable threshold on the coefficient magnitude, the wavelets representing noise and those representing the true signal can be separated. After separation, the coefficients below the threshold are made zero. On the basis of how the remaining coefficients are modified, the thresholding method may be termed as hard thresholding or soft thresholding.

In hard thresholding, the coefficients above the threshold are kept unmodified.

$$\hat{W}(m,n)=\begin{cases} W(m,n), & \left|W(m,n)\right|\geq\tau \\ 0, & \left|W(m,n)\right|<\tau \end{cases} \tag{2.26}$$

where τ is the threshold value. In soft thresholding, the threshold value is subtracted from the coefficients above the threshold.

$$\hat{W}(m,n)=\begin{cases} \operatorname{sgn}(W(m,n))(\left|W(m,n)\right|-\tau), & \left|W(m,n)\right|\geq\tau \\ 0, & \left|W(m,n)\right|<\tau \end{cases} \tag{2.27}$$

The waveform is reconstructed from the modified wavelet coefficients using the inverse wavelet transform (Eq. 2.17). Examples of hard and soft thresholding are shown in Fig. 2.6(a) and Fig. 2.6(b), respectively. The hard thresholding causes discontinuities in the wavelet domain. These discontinuities produce oscillations in the reconstructed signal. However, all the signal information is preserved if the threshold is suitably chosen. Soft thresholding does not cause discontinuities in the wavelet domain but the subtraction of the threshold value from the coefficients may cause loss of signal information. A compromise between the hard thresholding and soft thresholding is proposed in [25] for improved wavelet thresholding:

$$\hat{W}(m,n)=\begin{cases} \operatorname{sgn}(W(m,n))(\left|W(m,n)\right|-\tau\beta^{(\tau-\left|W(m,n)\right|)}), & \left|W(m,n)\right|\geq\tau \\ 0, & \left|W(m,n)\right|<\tau \end{cases} \tag{2.28}$$

where $\beta>1$. It approximates hard thresholding as $\beta\rightarrow\infty$ and it approximates soft thresholding as $\beta\rightarrow1$. The drawbacks of both hard and soft thresholding can be avoided by selecting an optimum value for β. Two other methods of a compromise between hard and soft thresholding are given in [26] as the following.

$$\hat{W}(m,n)=\begin{cases} \operatorname{sgn}(W(m,n))(\left|W(m,n)\right|-\alpha\tau), & \left|W(m,n)\right|\geq\tau \\ 0, & \left|W(m,n)\right|<\tau \end{cases},(0\leq\alpha\leq1) \tag{2.29}$$

$$\hat{W}(m,n)=\begin{cases} \operatorname{sgn}(W(m,n))\sqrt{(W(m,n))^2-\tau^2}, & \left|W(m,n)\right|\geq\tau \\ 0, & \left|W(m,n)\right|<\tau \end{cases} \tag{2.30}$$

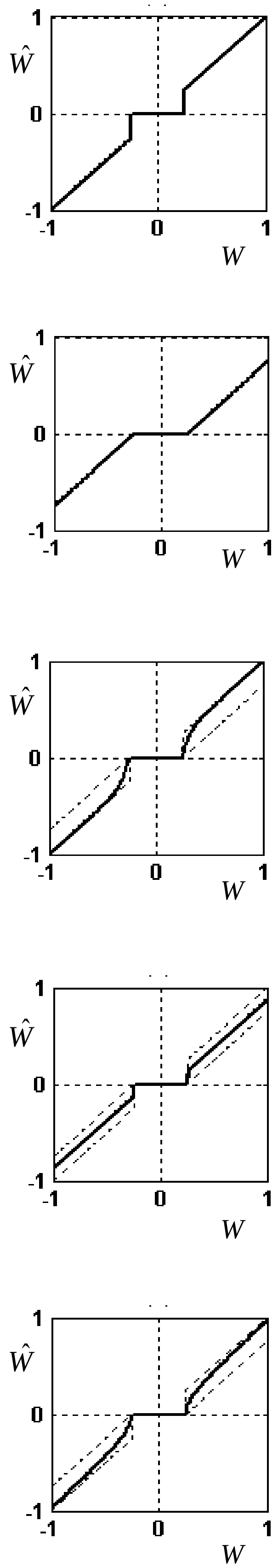

(a) hard thresholding, with τ = 0.25

(b) soft thresholding, with τ = 0.25

(c) improved thresholding of [25] as in Eq. 2.28, with τ = 0.25, β = 5

(d) improved thresholding of [26] as in Eq. 2.29, with τ = 0.25, α = 0.5

(e) improved thresholding of [26] as in Eq. 2.30, with τ = 0.25

Fig. 2.6. W vs $\hat{W}$ plots for different types of thresholding.

The modified soft thresholding methods of Eq. 2.28, 2.29, and 2.30 are graphically shown in figs. 2.6(c), 2.6(d), and 2.6(e) respectively. It is the choice of the threshold τ which determines the effectiveness of the thresholding based denoising method. For white Gaussian noise, Donoho *et al*. [23] suggested the use of a single threshold $\tau = \sigma\sqrt{2\log N}$ where σ^2 = noise variance and N = number of input samples. The best estimate of σ^2 can be obtained from $\mathbf{D}_1$ as it contains the highest frequency band and hence maximum number of wavelet coefficients representing noise. Another option for calculating the optimum threshold is Stein's unbiased risk estimator (SURE) [23]. In the context of ECG denoising, Zhang [22] observed that Donoho's single threshold causes over smoothing of the signal due to the high threshold value for the higher scale decomposition levels, and the SURE method results in insufficient noise suppression because of its low threshold value for the lower decomposition levels. Hence the empirical Bayes posterior median (EBPM) threshold method was used for setting optimum thresholds for lower as well as higher scale decomposition levels in the soft thresholding method based on Symlet 10 wavelet. The method was tested on a noisy ECG, sampled at 500 Hz, recorded from a dog. Denoising was found to be better for piecewise thresholding than that for processing the whole signal together.

Oscillations due to Gibbs phenomenon can occur at the sharp discontinuities in the waveform reconstructed using modified wavelet coefficients obtained either by linear wavelet filtering or by thresholding methods. If the discontinuity occurs at the quickly varying portion of the wavelet representing that region, the oscillation will have low amplitude. If the location of discontinuity is at a smooth portion of the wavelet, a high oscillation will result. To avoid this problem, Donoho and Coifman [27] proposed translation invariant denoising (TI denoising), consisting of the following steps:

1) The input noisy signal is circular shifted by m samples.
2) The shifted noisy signal is denoised using wavelet thresholding algorithm.
3) The denoised signal is shifted m samples in the opposite direction to cancel the shift.
4) Steps 1 to 3 are repeated by varying the value of m from 0 to M–1 to get M versions of the denoised outputs.
5) Average of the M denoised signals is taken as the final denoised signal.

The oscillations due to Gibbs phenomenon are different in the *M* denoised versions but the signal part will be the same. The oscillations get attenuated by averaging. The value of *M* is selected as the length of the wavelet dilated to the largest scale on which the thresholding is applied.

The TI denoising method was implemented to remove high frequency noise from the ECG signal in [22] and [25]. The beginning and end of the QRS complex in ECG signals are susceptible to Gibbs oscillations. In the simulation study conducted in [25], a noisy ECG signal was produced by mixing Gaussian noise with a clean ECG record from MIT/BIH database. For noisy ECG with input SNR of 17 dB, the improved thresholding of Eq.2.28 produced SNR improvement of 3.4 dB. Application of TI denoising algorithm produced 6.3 dB SNR improvement. In [22], high frequency noise was removed from the recorded ECG signal using TI denoising, and the denoised output did not show Gibbs oscillations. The major drawback of the TI denoising algorithm is its computational complexity.

2.5 Denoising using empirical mode decomposition (EMD)

In empirical mode decomposition (EMD) the signal is decomposed into a number of simple oscillations, namely intrinsic mode functions (IMF) [10],[28]-[33]. A waveform can be an IMF if it satisfies the following criteria:

a) The number of local maxima and the number of local minima differ by at most one.
b) The mean of the upper and lower envelop at any point is zero.

The IMFs are obtained from the input signal $\mathbf{x}$ using an algorithm called sifting, consisting of the following steps:

1) Set the iterating variable $i = 1$ and the first proto IMF $\mathbf{h}_0 = \mathbf{x}$.
2) Get all the local maxima and minima of the proto IMF $\mathbf{h}_{i-1}$.
3) Connect all the local maxima of $\mathbf{h}_{i-1}$ using a cubic spline to get an upper envelope $\mathbf{e}_u$. Similarly obtain the lower envelope $\mathbf{e}_l$. Calculate the mean of the two envelopes

$$\mathbf{m}_i = \left(\frac{\mathbf{e_u} + \mathbf{e_l}}{\mathbf{2}} \right) \tag{2.31}$$

4) Get the i^{th} proto IMF

$$\mathbf{h}_i = \mathbf{x} - \mathbf{m}_i \tag{2.32}$$

5) Evaluate the stopping criterion. One criterion can be the sum of difference (SD) defined as

$$\mathrm{SD} = \sum_{k=0}^{N} \frac{\left| h_{i-1}(k) - h_i(k) \right|^2}{h_{i-1}^2(k)} \tag{2.33}$$

where N is the length of the signal. If SD is above a preset threshold, increment the value of i and go to step 2. Otherwise go to the next step.

6) As the stopping criterion is satisfied take the $\mathbf{h}_i$ as IMF.

Once the IMF is obtained, it is subtracted from the input signal to get the residue $\mathbf{r}_1$.

$$\mathbf{r}_1 = \mathbf{x} - \mathbf{c}_1 \tag{2.34}$$

The residue may contain another IMF. Hence $\mathbf{r}_1$ is analyzed as the input signal to obtain the second IMF $\mathbf{c}_2$ and corresponding residue $\mathbf{r}_2$. The procedure is repeated until we get a residue $\mathbf{r}_J$ which is a constant, a monotonically increasing function, or a function with only one peak. Thus we decompose the signal into J IMFs ($\mathbf{c}_1$ to $\mathbf{c}_J$) and one residue $\mathbf{r}_J$, represented as

$$\mathbf{x} = \sum_{i=1}^{J} \mathbf{c}_i + \mathbf{r}_J \tag{2.35}$$

Though $\mathbf{r}_J$ is not an IMF, it is commonly referred to as the $(J+1)^{\text{th}}$ IMF for notation simplicity and Eq. 2.35 is represented as

$$\mathbf{x} = \sum_{i=1}^{J+1} \mathbf{c}_i \tag{2.36}$$

and thus the input signal is decomposed into a finite number of IMFs. Similar to the different scales of details in the wavelet decomposition, the IMF of different scales also represents different frequency bands of the signal. However, the frequency bands of different IMFs depend on the waveform being analyzed. The main advantage of EMD over wavelet-based decomposition is that it does not require a predefined basis function; it derives the basis function from the input waveform itself.

Boudraa and Cexus [29] reported an EMD based method to filter out the additive white Gaussian noise. The signal was decomposed into its component IMFs and the residue using EMD. The partial reconstructed signal $\tilde{\mathbf{x}}_k$ was obained for different values of k such that

$$\tilde{\mathbf{x}}_k = \sum_{j=k}^{J+1} \mathbf{c}_j \tag{2.37}$$

When actual signal **s** known, the value of k (say j_s) which achieves minimum mean square error (MSE) between **s** and $\tilde{\mathbf{x}}_{j_s}$ can be taken as the optimum value. For the practical cases, with the original signal not known, an empirical method for obtaining the value of j_s was developed. A distortion measure, called consecutive MSE (CMSE), was defined as

$$\text{CMSE}(\tilde{\mathbf{x}}_k, \tilde{\mathbf{x}}_{k+1}) = \frac{1}{N}\sum_{i=1}^{N} [\tilde{\mathbf{x}}_k(i) - \tilde{\mathbf{x}}_{k+1}(i)]^2 \tag{2.38}$$

where N is the length of the signal and k = 1, 2,…, J–1. From the CMSE values, the value of j_s can be obtained using the following equation

$$j_s = \underset{1 \le k \le N-1}{\arg\min} \left[\text{CMSE}\left(\tilde{\mathbf{x}}_k, \tilde{\mathbf{x}}_{k+1}\right) \right] \tag{2.39}$$

with the assumption that the initial IMFs up to j_s^{th} level contributes to the noise and the IMFs after j_s^{th} level contributes to the signal. The energy content in the j_s^{th} level IMF was minimum because, being the transition stage, it has minimum energy content of the noise and that of the signal. After getting the value of j_s, the optimum reconstructed signal $\tilde{\mathbf{x}}_{j_s}$ was obtained using Eq. 2.37.

The above method was evaluated using various computer simulated test signals. The input waveform **x** was obtained by adding Gaussian white noise $\mathbf{r}_0$ to the noise free signal **s** as in Eq. 2.23. Since the actual signal was known, it was possible to calculate the MSE value between the actual signal and the partial reconstructed signal $\tilde{\mathbf{x}}_k$ for different values of k. It was observed that minimum MSE was achieved by $\tilde{\mathbf{x}}_{j_s}$ for all the signals considered. The proposed method performed better than the windowing methods for all the signals considered, and it outperformed the wavelet method for some test signals. Application of the method as a signal from a fluid mechanics system showed that the EMD filtered output followed the trend of the signal.

An EMD based ECG denoising technique is reported in [10]. It was observed that the initial IMFs predominantly contain high frequency noise. The number of initial IMFs which contain significant amount of noise, p, was selected such that $\frac{1}{p}\sum_{k=1}^{p} \mathbf{c}_k = 0$ and $\frac{1}{p+1}\sum_{k=1}^{p+1} \mathbf{c}_k \neq 0$. It was not possible to remove these IMFs because they contain the QRS complex information also. To protect the QRS complexes, R-peak locations were obtained from the input ECG signal (the R-peak detection method was not reported). A series of Tukey windows (tapered cosine windows) of suitable widths were placed at R-peak locations of the first p IMFs. The values outside the windows were attenuated. When the signal was reconstructed using the modified IMFs, a good reduction in high frequency noise was observed. The baseline wander present in the signal was estimated from the IMFs using a filter bank. The baseline wander information was present in the final IMFs, with the low frequency components of the ECG signal. The baseline wander component was extracted from each of the IMFs using lowpass filters, starting from the residue ($(J+1)^{\text{th}}$ IMF). The cutoff frequency of the k^{th} lowpass filter which was used to filter the $(J-k+2)^{\text{th}}$ IMF is given by

$$\omega_k = \frac{\omega_0}{M^{k-1}} \tag{2.40}$$

where ω_0 is the cutoff frequency of the lowpass filter operated on the residue. $M > 1$ was called the frequency folding number. The baseline information extracted by the k^{th} filter was given by

$$\mathbf{b}_k = \mathbf{h}_k * \mathbf{c}_{J-k+2} \tag{2.41}$$

where $\mathbf{h}_k$ is the impulse response of the k^{th} filter. As the value of k increases, the baseline wander extracted by the filter decreases. This is measured by evaluating the variance of the extracted baseline wander. The authors defined a number called baseline wander order (q) which represents the number of IMFs from the last IMF those contain significant baseline wander information. Value of q was selected such that $\text{var}(\mathbf{b}_q) > \xi$ and $\text{var}(\mathbf{b}_{q+1}) < \xi$ where ξ is a suitably chosen threshold value. The total baseline estimate $\mathbf{B}$ is obtained by

$$\mathbf{B} = \sum_{i=1}^{q} \mathbf{b}_i \tag{2.42}$$

The baseline estimate is subtracted from the input ECG to get the baseline corrected output.

The performance of the processing was tested on noisy ECG, obtained by adding noise to clean ECG from MIT/BIH arrhythmia database and real noise records (which does not contain ECG) from the MIT/BIH noise stress test database. In the simulation studies, the authors used the Gaussian noise to simulate the high frequency noise, and used Gaussian pulses to simulate the baseline wander on records of 2000 samples with sampling rate of 360 Hz. The performance was compared to that of Butterworth filtering with lower and upper cutoff frequencies of 0.09 Hz and 30 Hz respectively. For an input noisy ECG with SNR = 10 dB, the signal-to-error ratio achieved by the EMD and filtering methods were 15.9 dB and 11.2 dB respectively. For further testing, recording of muscle artifact and the electrode motion artifact were added to the noise-free ECG signal. For different ECG records and different SNRs, the SER obtained by the EMD, Butterworth filtering, and the wavelet-based denoising were computed. The wavelet denoising method used 4-level wavelet transform using Cohen-Daubechies-Feauveau 9/7 wavelet. For various inputs with SNR = 6 dB, the EMD method achieved a SER of 8.9 – 11.5 dB, which was better than the SER achieved by Butterworth filtering (4.45 – 6.48 dB) and wavelet-based denoising (6.13 – 6.15 dB). The main drawback of the EMD based method is that it is computation intensive, and the cubic spline fitting often causes overflow and underflow. Since the cubic spline curve does not include the initial and final points, it may also cause oscillations at the beginning and ending of the IMFs. There is no direct procedure to find out the optimum value of the threshold for SD, which is used as a stopping criteria for the sifting process.

A combination of EMD decomposition and mathematical morphology filtering was used by Ji *et al.* in [30] to remove the baseline wander from the ECG signals. The authors used opening and closing, the two morphological operators defined in Eqs. 2.10 and 2.11 to extract baseline information from the i^{th} IMF as per the following equation.

$$\mathbf{b}_i = \frac{\left(\mathbf{c}_i \circ \mathbf{k_i} + \mathbf{c}_i \bullet \mathbf{k}_i\right)}{2} \tag{2.43}$$

where $\mathbf{c_i}$ is the i^{th} IMF. The structural element $\mathbf{k_i}$ is chosen as a flat (zero vector) with length of i^2. The extraction began from the last IMF ($(J+1)^{th}$ IMF, the residue) and stopped when the variance of the extracted baseline falls below a threshold. Finally, the baseline estimate is obtained as per the following equation.

$$B(t) = \sum_{i=m+1}^{J+1} b_i(t) \tag{2.44}$$

where $B(t)$ is the estimated baseline wander, m is such that the $\mathrm{var}(\mathbf{b_m}) < \xi$ and $\mathrm{var}(\mathbf{b_{m+1}}) > \xi$ where ξ is a suitably chosen threshold value. The method was validated using simulated studies, with the clean ECG from MIT/BIH arrhythmia database and the baseline simulated using a lowpass filtered random noise. The performance was quantified using correlation coefficient and the SNR improvement. It was observed that the performance of the proposed method was better than the mathematical morphological filtering method proposed in [15].

Kopsisnis and McLaughlin [31] applied thresholding techniques used in wavelet denoising, for EMD decomposed signals. Investigations to develop better sifting methods have also been reported [32]-[34].

2.6 Summary

Several denoising techniques including linear filtering, adaptive filtering, mathematical morphology filtering, spline interpolation, modified moving window averaging, ICA, and wavelet and EMD based processing have been reported for suppressing the baseline wander and motion artifact from the ECG signals. Among these techniques, wavelet-based denoising technique is found to be attractive because it does not require a reference signal as in adaptive filtering, multi-lead ECG record as in ICA, or information about the characteristic points as in interpolation methods. The EMD based processing, similar to wavelet-based processing, decomposes the signal into different scales. However, the band limits of decomposition scales obtained by EMD are not fixed, and depend on the noise content in the input signal. Hence it was decided to use wavelet-based processing for denoising of ECG signals. The details of the method and the results obtained are presented in the following two chapters.

Chapter 3
WAVELET-BASED DENOISING

3.1 Introduction

This chapter presents a wavelets based denoising technique for suppression of the motion artifact and baseline wander in the ECG signal. The advantage of wavelet-based method is that it does not require a reference signal, and it can be applied on a single-channel ECG. The wavelets Daubechies order 8 (db8), discrete Meyer (dmey), Symlets order 10 (sym10), Biorthogonal 6.8 (bior6.8) were investigated for the decomposition and subsequent denoising of the noisy signal. All the analysis and processing were carried out using Matlab.

The chapter begins with a description of the procedure for selecting an appropriate wavelet for the denoising application. This is followed by a description of the investigated denoising technique.

3.2 Test signals used for the study

Wavelet decomposition and denoising was studied using the following four groups of test signals.

1) The output from an ECG simulator (Phantom 320 [35]) acquired using a 12-bit DAQ unit. The simulator simulates ECG signals which are normal, abnormal, and with simulated artifacts. The sampling rate was set at 200 Hz.
2) The ECG recorded from volunteers using Holter ECG monitor developed at ECIL. The recordings were first taken with the subject sitting in an idle condition (without any voluntary movements). Subsequently the recordings were taken with the subject involved in moderate physical activities, commonly encountered during ambulatory ECG recording: hand movements, walking, and climbing stairs. The activities were chosen such that there was no significant change in the

cardiac activity. The instrument recorded 3-lead ECG, at a sampling rate of 200 Hz with 8-bit resolution.

3) The ECG records numbered 100, 103, 105, 111, 112, 113, 213, and 219 in the MIT/BIH arrhythmia database [36]. The records 111, 213, and 219 contain abnormalities like AV block, isolated peaks, and atrial fibrillation, while the rest of the recordings were clean and normal [37].
4) The records "bw", "ma", and "em" containing the baseline wander, muscle artifacts, and electrode motion artifact, respectively, in the MIT/BIH noise stress test database [36]. The noise recordings were obtained by placing the electrodes on the limbs in positions in which the ECG was not visible [38].

The actual record lengths varied from 20 s to 5 min, from which segments of 10 s duration were selected for the study. The records in MIT/BIH database were acquired at 360 Hz with 11-bit resolution. Sampling rate conversion was applied on these records to have all the test signals sampled at 200 Hz.

3.3 Selecting the appropriate wavelet

A large number of wavelet functions have been used in denoising applications. Some selected examples of wavelets and the corresponding scaling functions are shown in Fig. 3.1. When a waveform is analyzed using wavelets, the wavelet detail and approximation coefficients of scale *m* represent the correlation of the waveform with the scaled version of the wavelet $\Psi_m = 2^{-m/2}\Psi(2^{-m}t)\Phi$ and the scaling function $\Phi_m = 2^{-m/2}\Phi(2^{-m}t)$, respectively [12]-[14], [17]. The magnitudes of the coefficients measure the similarity between the waveform and the wavelet/scaling function. A component in the waveform having shape similar to the wavelet at scale *m*, is represented by the detail coefficients of scale *m*. To separate a signal from the noise, the wavelet is chosen such that the shapes of the wavelet or scaling function, at some scale, closely match the shape of the signal or noise. It is possible that the details of a particular scale capture the noise components in one scale and the signal components in another scale. For effective denoising, it is required to determine the detail and approximation levels which represents the signal component alone, the noise component alone, and both. Wavelet-based denoising is not very effective if most of the decomposition scales contain both signal and noise components.

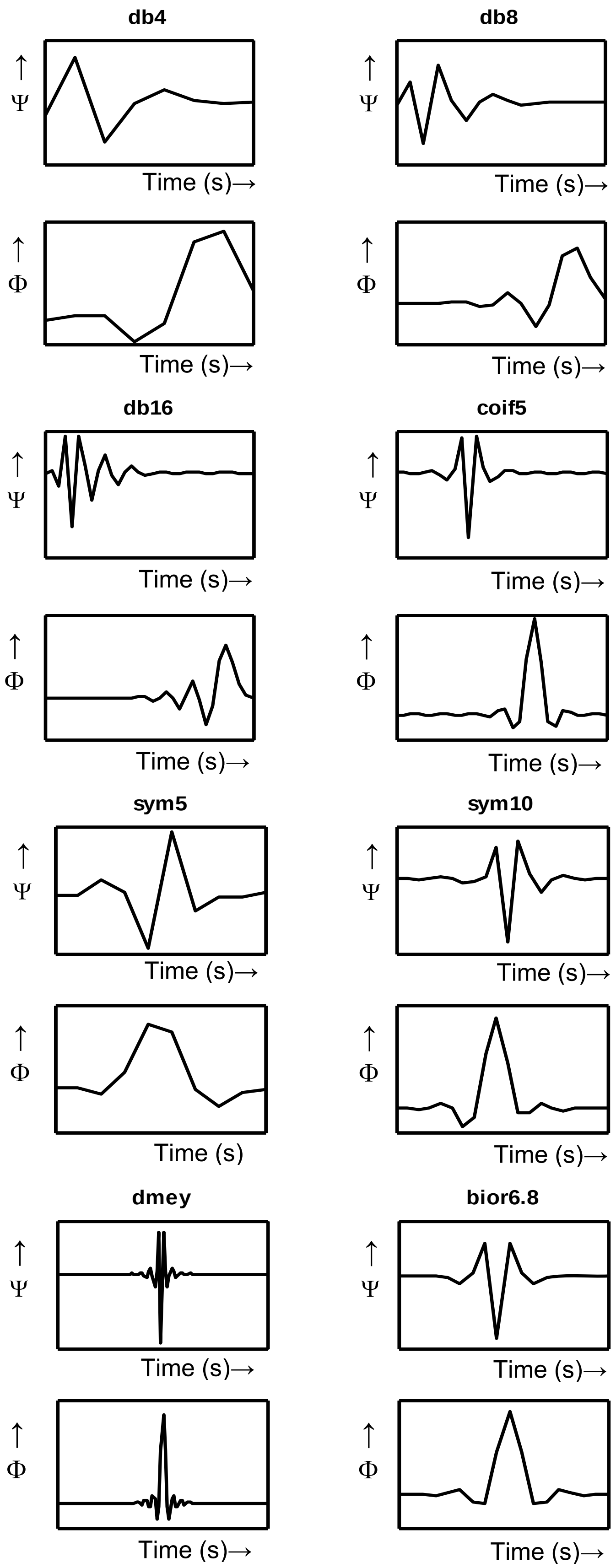

Fig. 3.1. Different wavelets and the curresponding scaling functions.

One example demonstrating the importance of the choice of wavelets can be seen in [17], which explored different types of wavelets (dmey, db6, and coif5) to decompose the ICG containing respiratory artifact. It was observed that the ICG signal was completely represented by the detail scales 1 – 8. The artifact was represented by 8th scale approximation. The other wavelets did not result in signal-artifact separation.

In case of ECG with baseline wander and motion artfact, the noise components do not have a characteristic shape. Hence, the similarity of the wavelet (or its scaling function) with the ECG signal is important. The wavelet should represent the ECG signal in minimum number of scales, separated from the initial and final scales. For this investigation, clean ECG signals were decomposed into 10 scales of details using different wavelets. The examples of decomposition levels obtained by sym5 wavelet and by dmey wavelet are given in Fig. 3.2 and Fig. 3.3 respectively. It can be observed that the amplitude of the initial decomposition levels D1 and D2 obtained by sym5 wavelet was more than that of the details obtained from dmey wavelet. It is preferred to have less amount of ECG content in D1 and D2, to attain a good separability from the high frequency noise present in the signal. It can also be noted that the details D5 to D7 obtained using sym5 have sharp peaks. However, the 5th to 7th scale details are expected to represent slow varying components similar to P-wave and T-wave of the ECG signal, which do not contain sharp peaks. An analysis

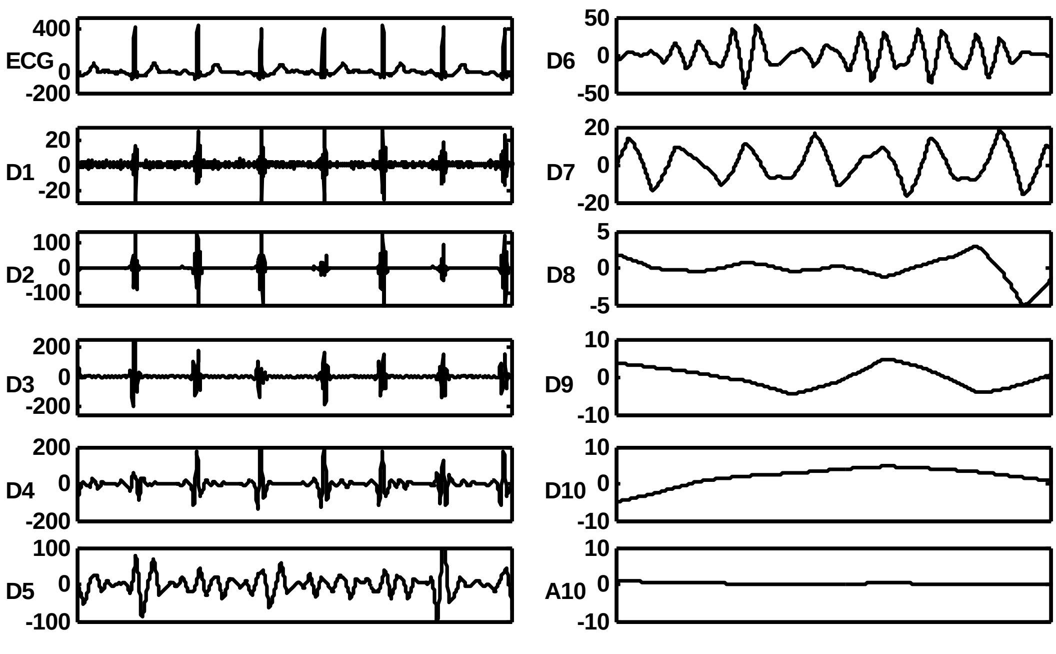

Fig. 3.2. Example of decomposition of ECG signals using Symlet 5 (sym5) wavelet. X- axis:Time duration of 6 s. Y-axis: amplitude (arbitrary units).

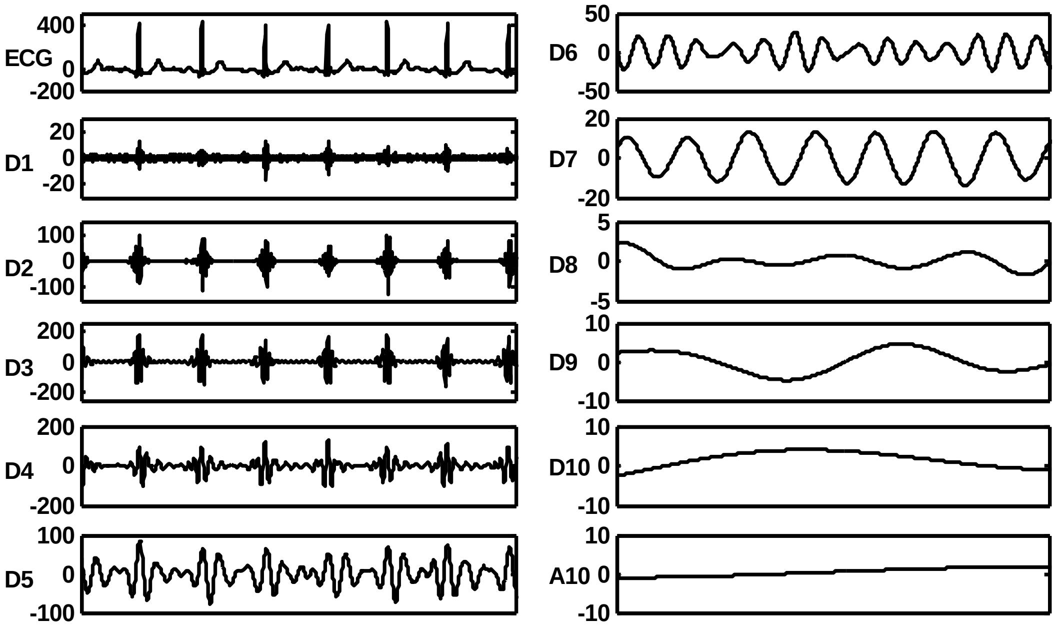

Fig. 3.3. Example of decomposition of ECG signals using discrete Meyer (dmey) wavelet. X- axis:Time duration of 6 s. Y-axis: amplitude (arbitrary units).

of the several signals showed similar results. Thus it can be concluded that dmey wavelet is a better choice to represent ECG signal compared to sym5 wavelet. The details and approximations obtained by the wavelets db8, sym10, and bior6.8 were similar to those obtained by dmey wavelet, and hence were chosen for detailed analysis.

3.4 The denoising method

To develop the denoising method, we need to know the decomposition levels with high presence of noise. A study was conducted on ECG segments of 10 s duration, sampled at 200 Hz. Out of 151 segments studied, 48 were clean ECG segments selected from records 100, 103, 112, 113, and 219 of MIT/BIH arrhythmia database. The rest 103 segments were selected from the ECG records obtained using the ECIL Holter ECG monitor. Out of these 103 segments, 37 were clean were artifact-free segments, and the remaining 66 were noisy segments, from the ambulatory recordings.

Each segment was decomposed into 9 levels using db8 wavelet, and the normalized RMS values of the details 1 to 9 were calculated as

$$\mathrm{RMS}_{i\mathrm{N}} = \frac{\mathrm{RMS}_i}{\sqrt{\sum_{i=1}^{9} \mathrm{RMS}_i^2}} \tag{3.1}$$

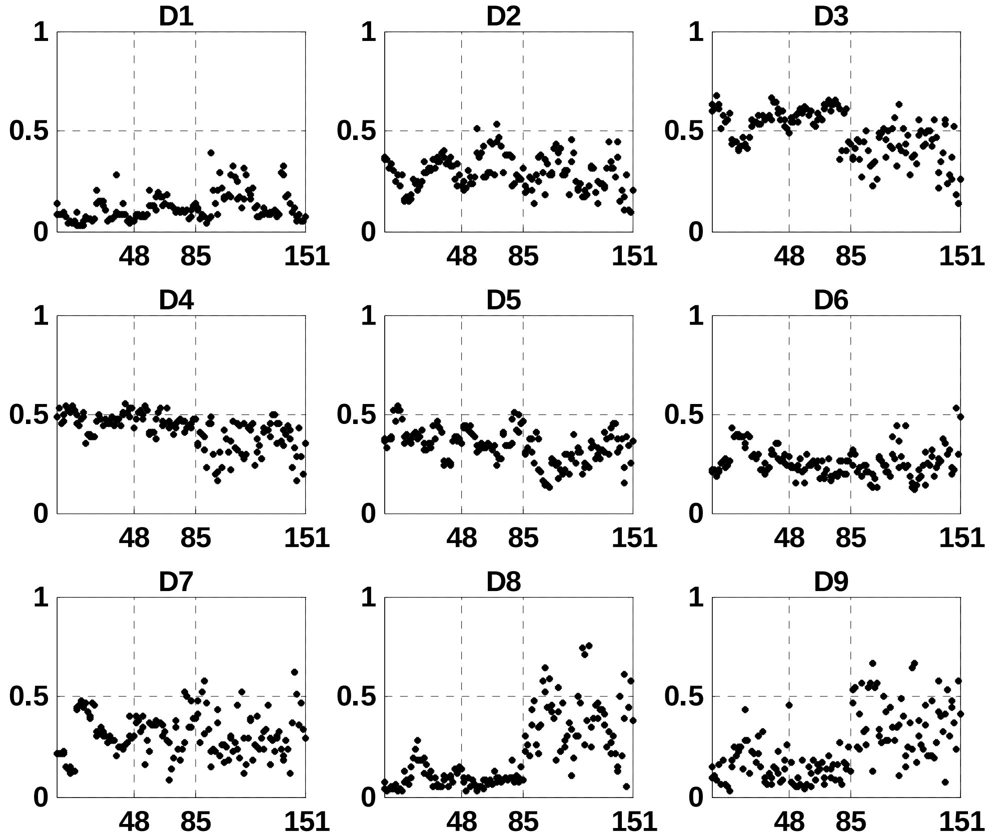

Fig. 3.4 RMS values of clean and noisy ECG segments of 10 s duration decomposed into details at different scales using db8 wavelet. X-axis: record numbers 1 to 151. Y-axis: normalized RMS values. Records 1-48: clean ECG segments of 10 s duration from MIT/BIH arrhythmia database. Records 49-85: clean ECG segments recorded using ECIL Holter ECG monitor. Records 86-151: noisy ECG segments recorded using ECIL Holter ECG monitor.

where RMS_i is the RMS value of i^{th} decomposition scale. The normalized RMS values obtained for the records at each scale are shown in Fig. 3.4. It can be observed that RMS values of the decomposition scales 1, 8, and 9 were low for clean ECG records and high for noisy ECG records. The RMS value of the decomposition levels 3, 4, and 5 reduced during the occurrence of noise, due to normalization.

It may be concluded that the decomposition scales 1, 8, and 9 contained low signal information and captured majority of the noise. The decomposition scales 3, 4, and 5 captured majority of the signal and a small amount of noise. The remaining decomposition levels had both signal and noise information. Thus, by reconstructing the signal using the decomposition levels 2 to 7, a considerable reduction of noise can be achieved. Hence we can use the following equation for obtaining the denoised signal $y(n)$ from input $x(n)$.

$$y(n) = \sum_{i=2}^{7} D_i(n) = x(n) - D_1(n) - A_7(n) \tag{3.2}$$

where $D_i(n)$ and $A_i(n)$ are the detail and approximation at i^{th} scale. The approximate bandwidth of $\mathbf{D}_1$ and $\mathbf{A}_7$ are 50 – 100 Hz and 0 – 0.78 Hz, respectively for input sampling rate = 200 Hz.

Chapter 4
TESTS AND RESULTS

4.1 Introduction

The ECG signals used for validating the denoising algorithm were obtained using a Holter ECG monitor from ECIL, Hyderabad, and ECG records from MIT/BIH database, as described earlier in Section 3.2. Effectiveness of the denoising technique was examined (i) qualitatively by visual examination of the processed output waveform, (ii) quantitatively by calculating improvement indices based on signal statistics, and (iii) by using it as a pre-processing for automated QRS detection. Denoising method and evaluation methods were implemented using Matlab 7.1.

Next section describes testing of the ECG monitor. The subsequent sections describe the validation methods and present the results.

4.2 Testing the ECG monitor

The Holter ECG monitor (from ECIL, Hyderabad) was tested using an ECG simulator "Phantom 320" [35]. The simulator output was recorded using (a) ECIL Holter ECG monitor, (b) Holter ECG monitor called "Locket" with an inbuilt ECG data acquisition system developed earlier at IIT Bombay [39], and (c) using DAQ unit "KUSB-3102" connected to USB port of a PC. The heights of the characteristic points of ECG from the isoelectric point and the widths of the QRS complexes and ST segments were measured for all the three methods of recording. It was found that the recorded signals and the acquired signal have the same statistics, despite slight differences caused by the quantization error. The ECIL instrument was then used to record the ECG from healthy volunteers with no known cardiac disorders under ambulatory conditions. The ECG recordings from the same volunteers under nearly identical conditions were also recorded using the IITB Holter ECG monitor for comparison. The two instruments exhibited very similar artifacts.

4.3 Application of denoising on simulated ECG

The denoising was first applied on clean ECG signal acquired from the simulator, to assess any signal distortions due to denoising process. An example of the processing is shown in Fig. 4.1. The processing removes the DC component of the input signal which can be seen as a shift of the isoelectric level. There is no other visible change in the processed output. However, in the processed outputs of clean ECG segments of beat-rate outside 45 – 150 range, some distortions were visible. The SER values were calculated for processing of simulator outputs with of beat-rates varied over 45 – 150 beat/min, and it ranged 18 – 28 dB (average = 22.5 dB, s. d. = 3.5 dB).

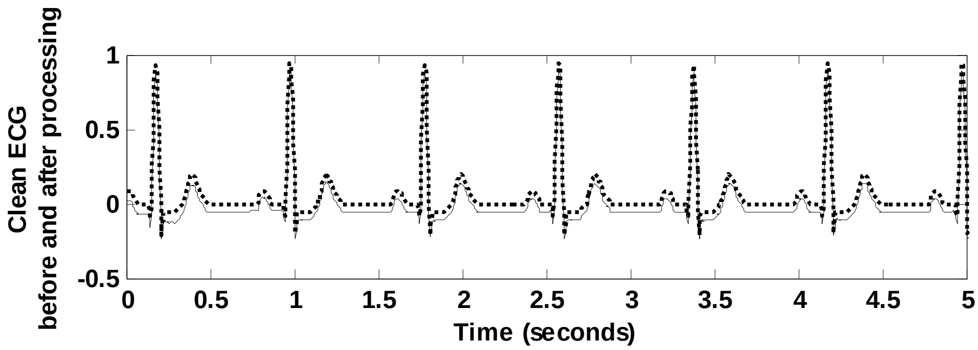

Fig. 4.1. Clean ECG from the simulator (dotted line) and the output obtained after wavelet denoising (continuous line).

4.4 Qualitative examination of denoising

The denoising technique was applied on segments in the ambulatory ECG from healthy volunteers, recorded using ECIL Holter ECG monitor. An example of the denoising is shown in Fig. 4.2. It shows a noisy ECG segment and the outputs obtained after denoising using different wavelets and the output from a 500-tap bandpass FIR filter with pass-band of 0.78 – 50 Hz.

The input segment has EMG noise in the region of 4 – 6 s and baseline wander in the region of 7 – 9 s. A considerable reduction in the baseline wander can be observed in all the outputs, although there is no significant reduction in EMG noise. It may be noted that some of the isoelectric regions (*e. g.*, at 7 and 8 s) of the denoising output using sym10 and bior6.8 are not flat. The magnitude spectra of the waveforms, as shown in Fig. 4.3, were also examined. The FIR filter has the minimum transition band and produces maximum attenuation to the high frequency components above 50 Hz. Among wavelets, dmey wavelet has the minimum transition band. However, db8 wavelet produced more attenuation to the high frequency components above 75 Hz than all other wavelets considered. From the initial part of the spectrum shown in Fig. 4.4, it can be noted that the noisy ECG contains high magnitudes of low frequency components in the range 0 – 1 Hz,

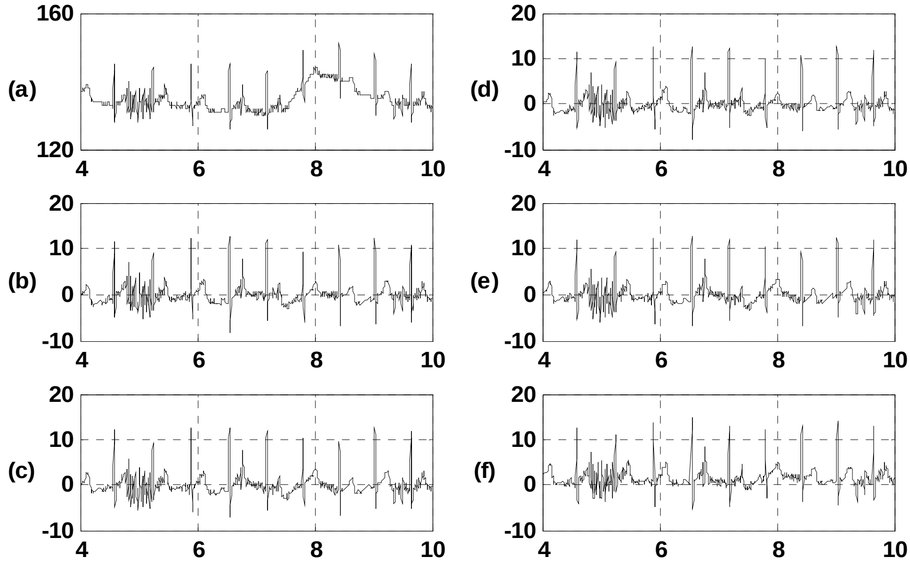

Fig. 4.2. (a) Noisy ECG signal. (b)-(e) The output obtained after wavelet-based processing using db8, sym10, dmey, and bior6.8 wavelets respectively. (f) The output obtained after 500-tap FIR filtering. X-axis: time (s), Y-axis: amplitude (arbitrary unit)

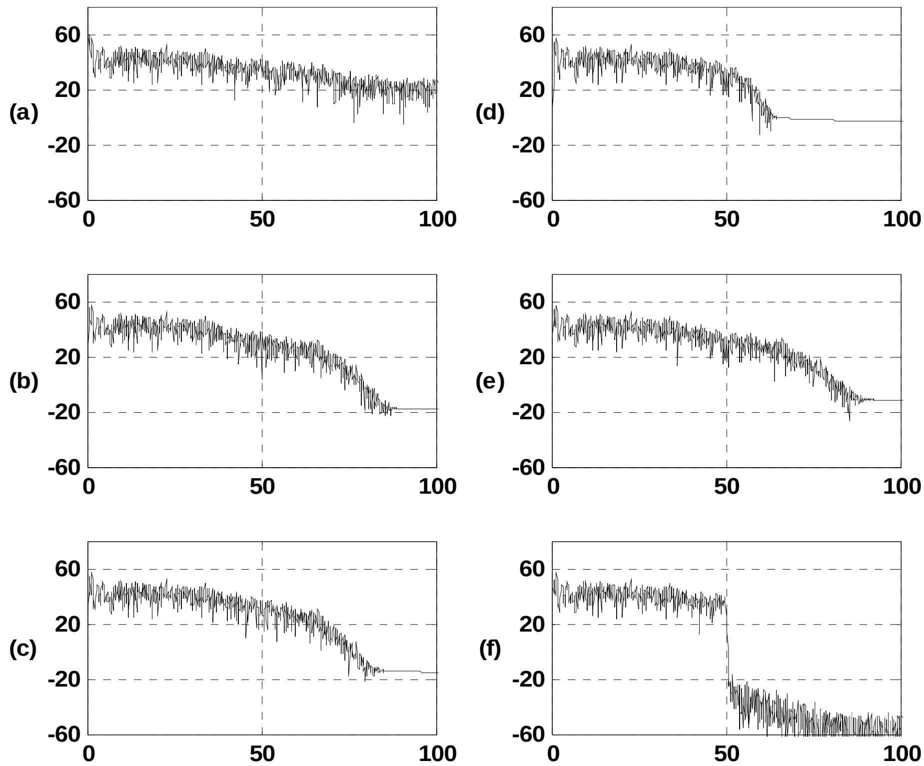

Fig. 4.3. The magnitude spectrum of (a) noisy ECG, (b)-(e) The output obtained after wavelet-based processing using db8, sym10, dmey, and bior6.8 wavelets respectively, and (f) The output obtained after 500-tap FIR filtering. X-axis: frequency (Hz), Y-axis: amplitude (dB)

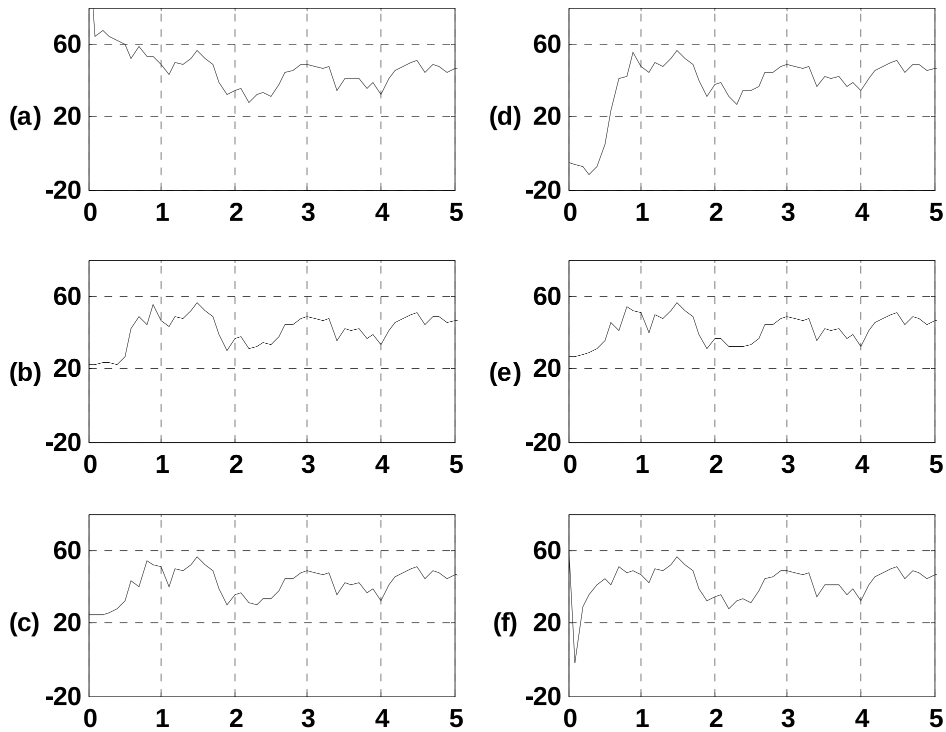

Fig. 4.4. The zoomed magnitude spectrum of (a) noisy ECG, (b)-(e) the output obtained after wavelet-based processing using db8, sym10, dmey, and bior6.8 wavelets respectively, and (f) the output obtained after 500-tap FIR filtering. X-axis: frequency (Hz), Y-axis: amplitude (dB).

representing significant baseline wander. These components were attenuated in the processed waveforms. The dmey and db8 wavelets give sharper transition bands compared to other wavelets. All the frequency components below 0.5 Hz were largely attenuated by dmey wavelet. The 500-tap FIR filter has slow transition and removes only the very low frequency components.

Application of the denoising technique on noisy segments from the MIT/BIH database gave similar results.

4.5 Quantification of signal enhancement

The validation method reported in [4] was used to quantify the noise reduction achieved by the denoising algorithm. The ECG records obtained from the volunteers using ECIL Holter ECG monitor were used for the purpose. The clean segments of the records which did not contain artifacts were visually selected and were taken as noise-free ECG records. The denoising was applied on the noisy segments from the same record. The effectiveness of the filtering was quantified by calculating the L_2 norm and MaxMin statistic (Eqs. 2.1 and 2.2). The statistics were calculated for noisy signal before processing, after processing, and the ECG recorded without artifact.

Improvement indices for L_2 and L_{mxmn} were calculated as given in Eq. 2.3. An improvement index close to 1 indicates an effective denoising. The average values obtained for the improvement indices for different wavelets and FIR band-pass filtering are shown in Table 4.1. The indices show significant reduction of noise. These values show nearly the same improvement by all the denoising methods.

Table 4.1. Average values of the improvement indices obtained using different wavelets.

Process	**Improvement index**	
	L_2 Norm	**MaxMin**
db8	0.72	0.51
bior6.8	0.71	0.55
coif5	0.71	0.55
sym10	0.71	0.53
dmey	0.71	0.54
db4	0.71	0.54
BP filter	0.71	0.54

Signal enhancement was quantified by measuring SNR improvement also. The input signals used for this study were obtained by adding noise-free ECG segments

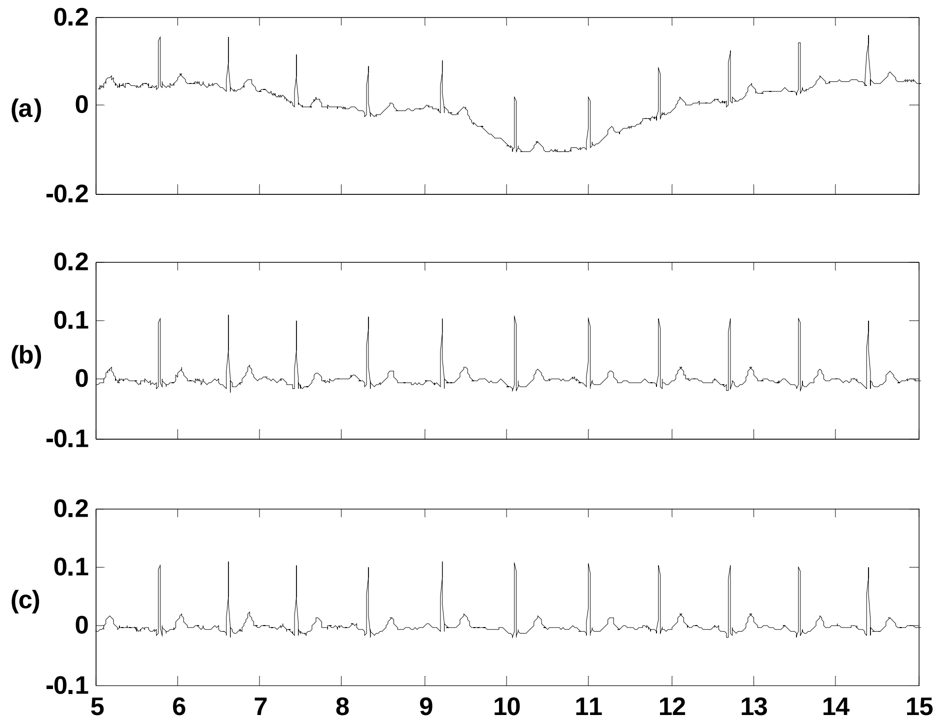

Fig. 4.5. (a) An ECG record with SNR = -5 dB obtained by adding segments from records "bw" and 100 from MIT/BIH database. (b) Output after wavelet denoising (db8). (c) Output after 500-tap FIR band-pass filtering.

from MIT/BIH arrhythmia database and signal-free noise segments from MIT/BIH noise stress test database. Example of an ECG signal with SNR = –5 dB is shown in Fig. 4.5(a). This waveform is synthesized by mixing segments of records 100, and "bw" from MIT/BIH database. The processed outputs obtained by wavelet denoising, using db8 wavelet, and FIR filtering are given in Figs. 4.5(b) and (c) respectively. It can be noted that the baseline wander has been significantly reduced. SER values achieved by different wavelets and FIR band-pass filtering for different combinations of ECG and noise records are given in Table 4.2, for the SNR values of 0 and 15 dB. It can be noted that the denoising technique under study is effective in suppressing the baseline wander but there is no significant suppression of muscle artifact and electrode motion artifact. Here also it is visible that the wavelet-based and the filter based denoising shows similar performance.

Table 4.2. SER values (in dB) for different types of noises

Noise	**ECG Rec.**	**SNR = 0 dB**			**SNR = 15 dB**		
		db8	**dmey**	**BP filter**	**db8**	**dmey**	**BP filter**
"bw"	100	13.82	14.05	13.91	15.44	15.71	15.81
	103	15.14	15.60	15.12	17.62	18.19	18.23
	213	15.19	15.74	15.14	17.86	18.48	18.56
"em"	100	7.88	7.88	8.44	14.87	15.09	15.25
	103	8.09	8.07	8.63	15.84	16.15	16.26
	213	8.34	8.23	8.83	17.10	17.38	17.66
"ma"	100	3.12	3.15	3.16	13.70	13.91	13.94
	103	3.16	3.20	3.22	14.36	14.65	14.68
	213	3.24	3.26	3.29	15.22	15.52	15.63

Figure 4.6 shows the SER vs. SNR plot obtained for different combinations of record 100 and record "bw". It is possible that the baseline wander already present in record 100 affected the results. Another evaluation was carried out by mixing the "bw" record with the artifact-free ECG signal, with beat rate 75, from the simulator. The SER vs. SNR plot obtained from this input is given in Fig. 4.7. From both the figures, it was observed that for input SNR of –10 dB, the denoising based on "db8" and "dmey" wavelets provided about 1 dB more signal to error ratio than the other wavelets used.

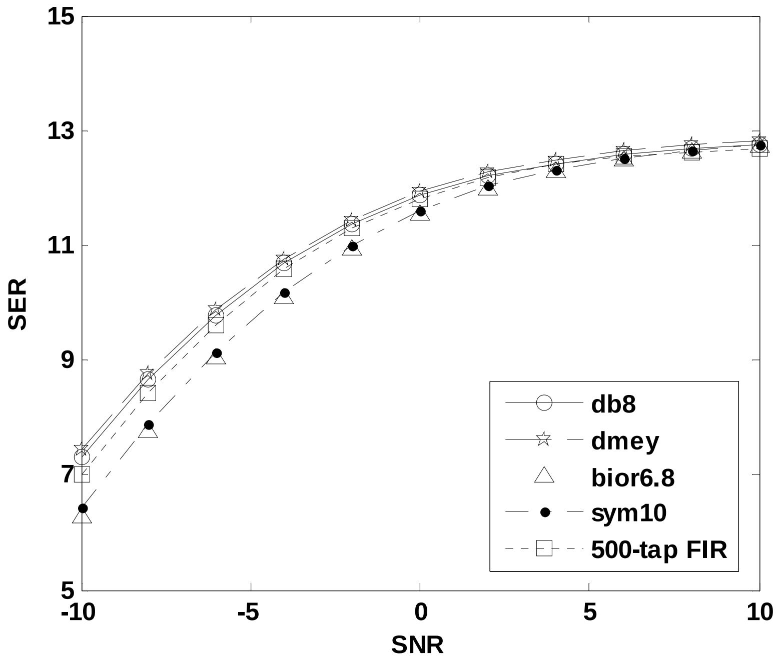

Fig. 4.6. SER versus SNR values (in dB) for wavelet-based decomposition and FIR band-pass filtering. The input signals were obtained by adding segments from records 100 and "bw" from MIT/BIH database.

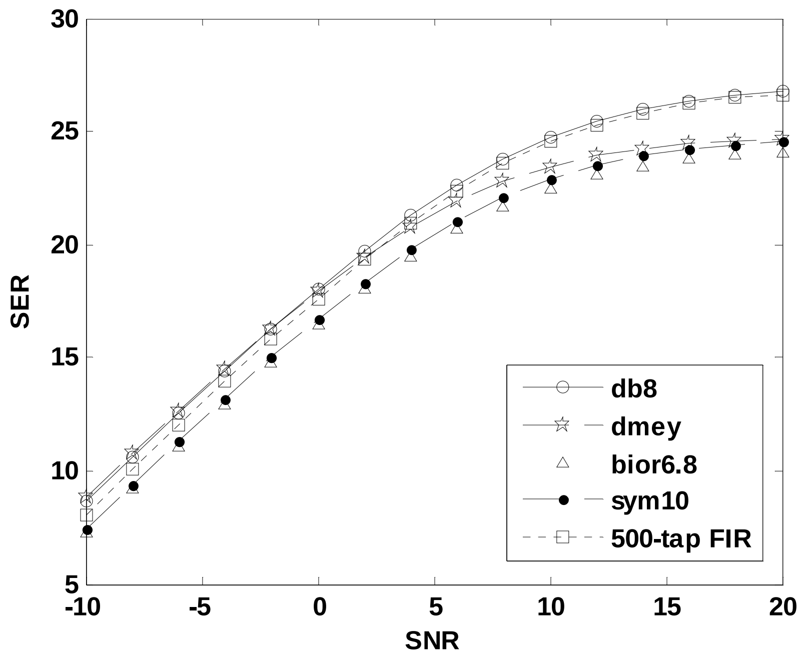

Fig. 4.7. SER versus SNR values (in dB) for wavelet-based decomposition and FIR band-pass filtering. The input signals were obtained by adding segments from clean ECG record acquired from simulator and record "bw" from MIT/BIH database.

4.6 Validation by QRS detection

For further assessing the baseline correction and noise reduction by the denoising technique, it was used as a pre-processing step to an automated QRS detection algorithm. The Pan-Tompkin's algorithm [3], [8], [9] for detecting the QRS complex was used to detect the R-peaks of the ECG records before and after denoising and improvements in the QRS detections were examined.

Pan and Tompkins [8] developed a robust QRS detection algorithm for real-time processing of ECG signals sampled at 200 Hz. It was implemented using an 8-bit microprocessor and hence the filters were designed with integer coefficients. The block diagram describing the algorithm is given in Fig. 4.8. The algorithm makes use of a bandpass filtering with the pass-band of around 5 – 15 Hz to attenuate the high frequency noise, baseline wander and the ECG components other than the QRS complex. The resulting signal is passed though a series of operations: differentiation, squaring, and moving window integration. The output obtained from the moving window integrator was used to find the R-peak locations and the widths of the QRS complexes.

Low-pass filter used has a cut-off frequency of 11 Hz. The difference equation of the filter,

$$y(n) = 2y(n-1) - y(n-2) + x(n) - 2x(n-6) + x(n-12) \tag{3.3}$$

It has a DC gain of 36 and a delay of 6 samples. The lowpass filter output was applied as input to a highpass filter with cut-off frequency 5 Hz and a gain of 32, with the difference equation

$$y(n) = 32x(n-16) - \left[y(n-1) + x(n) - x(n-32)\right] \tag{3.4}$$

It produces a delay of 16 samples. The QRS complex slope information is obtained by taking 5-point derivative, using the difference equation

$$y(n) = \frac{1}{8T}\left[-x(n-2) - 2x(n-1) + 2x(n+1) + x(n+2)\right] \tag{3.5}$$

It produced a delay of 2 samples. The differential signal is squared and then passed through the moving window integrator of length *N*, using the difference equation

$$y(n) = \frac{1}{N}\left[-x(n-(N-1)) - 2x(n-(N-2)) + ... + x(n)\right] \tag{3.6}$$

Selecting $N = 30$ resulted in 150 ms window length, spanning the QRS complex even in the abnormal conditions, and excluding the T wave from the QRS complex. The presence of the QRS complex is indicated when the moving integrator output crosses a threshold value, dynamically adjusted for an efficient R-peak detection.

For our investigation, a real-time implementation of the algorithm was not needed. A fixed threshold of magnitude equal to 50 % of the maximum value of the moving window integrator output was used. With this threshold, R-peak locations could be successfully detected in the clean ECG records. However, it failed to detect some R-peaks in noisy ECG records.

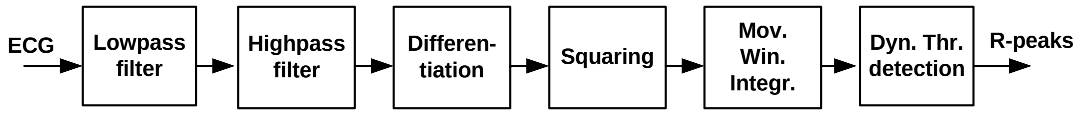

Fig. 4.8. The block diagram of the processing stages in Pan-Tompkin's algorithm [3], [8], [9].

4.7 Effect of denoising on QRS detection

One example of the validation using the Pan-Tompkin's algorithm is shown in Fig. 4.9. In the unprocessed ECG record, shown in Fig 4.9(a), there are several QRS complexes which the Pan-Tompkin's algorithm failed to detect. However, the algorithm was able to detect a much larger number of the R-peaks from the processed ECG record, as shown in Fig. 4.9(b) and (c). It is seen that the processing did not help in detecting the undetected peaks in some instances, but there were no instances of failure in the detections of R-peaks due to processing.

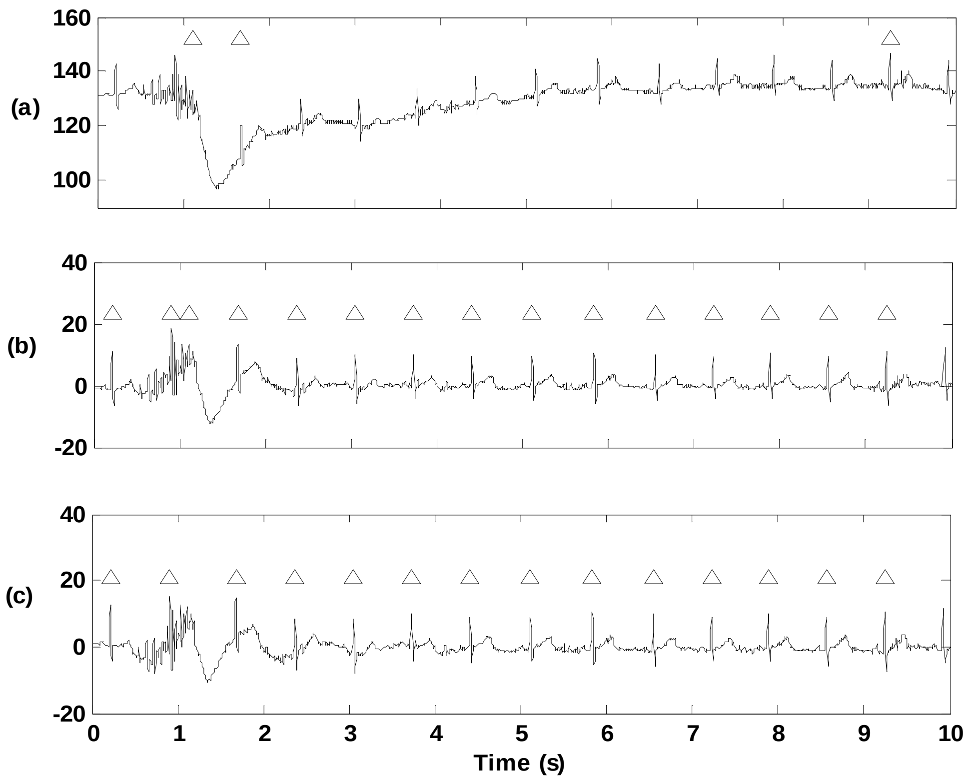

Fig. 4.9. (a) The recorded ECG from a volunteer during arm movement. (b) ECG after FIR band-pass filtering. (c) ECG after wavelet denoising. Triangles represent the detected QRS complexes by Pan-Tompkin's algorithm.

Chapter 5
SUMMARY AND CONCLUSION

The objective of this project was to investigate denoising techniques for suppressing motion artifacts and baseline wander in the ECG signals. After a study of various techniques, the wavelet-based denoising using scale-dependent thresholding was chosen for detailed investigation because it did not require a reference signal and can be used for single channel ECG records. By observing the decomposed waveforms of clean ECG signal using several wavelets, it was concluded that db8, dmey, sym10, and bior6.8 were suitable for the application, as they represent ECG signal in minimum number of decomposition levels. The RMS values of the various scales of details were calculated for clean and noisy ECG signals. It was found that the decomposition scales 1, 8, and 9 had low RMS values for clean ECG records and high RMS values for noisy ECG records. Hence those scales were eliminated. This denoising method was applied to clean ECG records, of different beat rates, obtained from the simulator and observed that it does not cause any significant distortion in the signals with beat-rate within the range 45 – 120. The method was tested for a large number of noisy signals and was found to eliminate the baseline wander very efficiently. An FIR band-pass filter was also investigated and it showed somewhat similar denoising effect. The methods were validated by calculating the improvement indices for the L_2 norm and MaxMin statistics. The values obtained shows significant denoising. Pan Tompkins QRS complex detection algorithm [8] was implemented and applied for QRS detection of the noisy and denoised signals. Denoising significantly improved the QRS detection efficiency of the algorithm.

The results from the investigation on wavelet based denoising show scope for several investigations to further improve the denoising. In the investigated method, the details at scales containing significant signal information were unmodified. However, those decomposition levels are not free from the artifacts. The possibility of separating the signal and noise components from these levels may also be explored. Another way of approaching the problem is to investigate the use of combination of two types of denoising techniques. For example, output of the wavelet-based denoising can be used for the detection of QRS complexes. The information of the R-peak locations obtained from this step can be used in the modified averaging method [7] for estimating and suppressing the baseline wander, or it can be used for generating the reference in the adaptive filtering technique of [12] or for protecting the QRS segments in the EMD technique [10]. Once the signal is enhanced to the extent that P waves can be successfully detected, we can use the adaptive filtering techniques needing the length of the PQRS complex [12]. Further there is a need for a quantitative evaluation of the various techniques on the same database, for carrying out a comprehensive comparison and selecting the best methods for the denoising of ambulatory ECG.

REFERENCES

[1] A. C. Guyton, *Textbook of Medical Physiology*, 7th ed., Saunders, Philadelphia, PA, 1986.

[2] W. H. Olson, "Basic concepts of medical instrumentation," in *Medical Instrumentation, Application and Design,* J. G. Webster (Editor), Houghton Mifflin, Boston, MA, 1992.

[3] W. J. Tompkins, *Biomedical Digital Signal Processing*, Prentice Hall, New Delhi, 1995.

[4] D. A. Tong, K. A. Bartels, and K. S. Honeyager, "Adaptive reduction of motion artifact in the electrocardiogram," in *Proc. 2nd Joint Conf. EMBS/BMES*, Houston, Texas, 2002, vol. 2, pp. 1403 – 1404.

[5] T. He, G. Clifford, and L. Tarassenko, "Application of ICA in removing artefacts from the ECG," *Neural Comput. and Appl.*, vol. 15, pp. 105 – 116, 2006.

[6] S. V. Pandit, "ECG baseline removal through STFT," in *Proc. 18th Int. Conf. IEEE/EMBS*, Amsterdam, 1996, pp. 1405 – 1406.

[7] M. Dai and S. Lian, "Removal of baseline wander from dynamic electrocardiogram signals," in *Proc. 2nd Int. Congr. Image Sig. Proc.*, Tianjin, China, 2009, pp. 1 – 4.

[8] J. Pan and W. J. Tompkins, "A real-time QRS detection algorithm," *IEEE Trans. Biomed. Eng*., vol. 32, pp. 230 – 236, 1985

[9] P. S. Hamilton and W. J. Tompkins, "Quantitative investigation of QRS detection rules using the MIT/BIH arrhythmia database," *IEEE Trans. Biomed. Eng*., vol. 33, pp. 1157 – 1165, 1986.

[10] M. Blanco-Velasco, B. Weng, and K. E. Barner, "ECG signal denoising and baseline wander correction based on the empirical mode decomposition," *Comput. Biol. Med.*, vol. 38, pp. 1 – 13, 2008.

[11] J. A. Van Asté and T. S. Schilder, "Removal of base-line wander and power-line interference from the ECG by an efficient FIR filter with a reduced number of taps," *IEEE Trans. Biomed. Eng.*, vol. 32, pp. 1052 – 1060, 1985.

[12] N. V. Thakor and Y. S. Zhu, “Application of adaptive filtering to ECG analysis: Noise cancellation and arrhythmia detection,” *IEEE Trans. Biomed. Eng.,* vol. 38, pp. 785 – 794, 1991

[13] C. Meyer and H. N. Keiser, “Electrocardiogram baseline noise estimation and removal using cubic splines and state-space computation techniques,” *Comput. Biomed. Res.,* vol. 10, pp. 459 – 470, 1977.

[14] C. H. Chu and E. J. Delp, “Impulsive noise suppression and background normalization of electrocardiogram signals using morphological operators,” *IEEE Trans. Biomed. Eng.*, vol. 36, pp. 262–273, 1989.

[15] P. Sun, Q. H. Wu, A. M. Weindling, A. Finkelstein, and K. Ibrahim, "An improved morphological approach to background normalization of ECG signals," *IEEE Trans. Biomed. Eng.*, vol. 50, pp. 117 – 121, 2003.
[16] S. G. Mallat, "A theory of mutiresolution signal decomposition: The wavelet representation," *IEEE Trans. Pattern Anal. Mach. Intell.*, vol. 11, pp. 674 – 693, 1989.
[17] C. K. Chui, *An Introduction to Wavelets*, Academic Press, London, 1992.
[18] C. Blatter, *Wavelets A Primer*, Universities Press, Hyderabad, India, 2003.
[19] K. Q. Wang, L. S. Xu, L. Wang, Z. G. Li, and Y. Z. Li, "Pulse baseline wander removal using wavelet approximation," *Comput. Cardiol.,* 2003, pp. 605 – 608.
[20] L. S. Xu, D. Zhang, and K. Q. Wang, "Wavelet-based cascaded adaptive filter for removing baseline drift in pulse waveforms," *IEEE Trans. Biomed. Eng.*, vol. 52, pp. 1973 – 1975, 2005.
[21] V.K. Pandey and P.C. Pandey, "Wavelet-based cancellation of respiratory artifacts in impedance cardiography," *Proc. 15th Int. Conf. Digital Signal Processing (DSP 2007)*, Cardiff, UK, 2007, pp. 191 – 194.
[22] D. Zhang, "Wavelet approach for ECG baseline wander correction and noise reduction," in *Proc. 27th Int. Conf. IEEE/EMBS*, Shanghai, China, 2005, pp. 1212 – 1215.
[23] D. L. Donoho and I. M. Johnstone, "Threshold selection for wavelet shrinkage of noisy data," in *Proc. 16th Int. Conf. IEEE/EMBS*, Baltimore, MD, 1994, vol. 1, pp. A24 – A25.
[24] D. L. Donoho, "De-noising by soft-thresholding," *IEEE Trans. Inform. Theory*, vol. 41, pp. 613 – 627, 1995.
[25] L. Su and G. Zhao, "De-noising of ECG signal using translation-invariant wavelet de-noising method with improved thresholding," in *Proc. 27th Int. Conf. IEEE/EMBS*, Shanghai, China, 2005, pp. 5946 – 5949.
[26] S. Guoxiang and Z. Ruizhen, "Three novel models of threshold estimator for wavelet coefficients," in *Lecture Notes in Computer Science: Wavelet Analysis and Its Applications*, Y. Y. Tang *et al*. (Eds), Springer-Verlag, Berlin, vol. 2251, pp. 145 – 150, 2001.
[27] R. R. Coifman and D. L. Donoho. "Translation-invariant de-noising." in *Springer Lecture Notes in Statistics*: *Wavelets and Statistics*, A. Antoniadis and G. Oppenheim (Eds.), Springer Verlag, New York, vol. 103, pp. 125 – 150, 1994.
[28] N. E. Huang, Z. Shen, S. R. Long, M. C. Wu, H. H. Shih, Q. Zheng, N.-C. Yen, C. C. Tung, and H. H. Liu, "The empirical mode decomposition and the Hilbert spectrum for nonlinear and non-stationary time series analysis," *Proc. Mathematical, Physical and Engineering Sciences*, The Royal Society, Vol. 454, pp. 903 – 995, 1998.
[29] A. -O. Boudraa and J. -C. Cexus, "EMD-based signal filtering," *IEEE Trans. Instrum. Meas.*, vol. 56, pp. 2196 – 2202, 2007.
[30] T. Y. Ji, Z. Lu, Q. H. Wu, Z. Ji, "Baseline normalisation of ECG signals using empirical mode decomposition and mathematical morphology," *Electronic Letters*, vol. 44, pp. 82 – 83, 2008.
[31] Y. Kopsinis and S. McLaughlin, "Development of EMD-based denoising methods inspired by wavelet thresholding," *IEEE Trans. Sig. Proc.*, vol. 57, pp. 1351 – 1362, 2009.
[32] B.Xuan, Q.Xie, and S. Peng, "EMD sifting based on bandwidth," *IEEE Signal Process Lett.*, vol. 14, pp. 537 – 540, 2007.

[33] S. Meignen and V. Perrier, "A new formulation for empirical mode decomposition based on constrained optimization," *IEEE Signal Process Lett.*, vol. 14, pp. 932 – 935, 2007.
[34] E. Deléchelle, J. Lemoine, and O. Niang, "Empirical mode decomposition: an analytical approach for sifting process," *IEEE Signal Process Lett.*, vol. 12, pp. 764 – 767, 2005.
[35] Müller and Sebastiani Elektronik GmbH, "Phantom 320 ECG simulator," available online, http://www.ms-gmbh.de/en/phantom_start.htm, Accessed on 21st Feb. 2010.
[36] Physionet, "PhysioBank ATM", available online, http://www.physionet.org/ cgi-bin/ATM.
[37] Physionet, "The MIT-BIH arrhythmia test database", available online, http:// www.physionet.org/physiobank/database/mitdb.
[38] Physionet, "The MIT-BIH noise stress test database", available online, http://www.physionet.org/physiobank/database/nstdb.
[39] M. Shojaei-Baghini, R. K. Lal, and D. K. Sharma, “A low-power and compact analog CMOS processing chip for portable ECG recorders,” in *Asian Solid State Circuit Conference, A-SSCC’05*, Hshinchu, Taiwan, Nov. 2005.

ACKNOWLEDGEMENT

I am grateful to Prof. P. C. Pandey for giving me an opportunity to work under his esteemed guidance for my M. Tech Project. I would like to express my deep gratitude for his valuable suggestions and constant encouragement throughout the project. I thank Prof. S. Mukherji for providing the ECG simulator for the project and other supports.

I thank Dr. Vinod Pandey for the support during signal recordings and his critical inputs on the dissertation. I am thankful to Mr. Prashant K. Mishra of ECIL for help in using the ECIL Holter ECG monitor and insightful inputs.

I would also like to express my sincere thanks to all my labmates for their unstinted help, support and guidance during the project work. I am also thankful to my batchmates, Ankita, Suresh, and Mahendra for making the life in IIT unforgettable.

I am highly indebted to my parents and Sreehari for all the moral support during my studies.

P. Mithun

29th June 2010